ENTECH '22

VIII. INTERNATIONAL ONLINE ENGINEERING AND TECHNOLOGY CONFERENCE PROCEEDINGS

ENTECH ’22

ENTECH '22 / VIII. International Online Engineering and Technology Conference PROCEEDİNGS

ISBN: 978-625-7034-28-9

Özgür Öztürk DAKAM YAYINLARI

December 2022, Istanbul, Turkey.

www.dakam.org

Firuzağa Mah. Boğazkesen Cad., No:76/8, 34425, Beyoğlu, İstanbul

Cover Photo: Photography is by Adrian Deweerdt. Project credits: Frank Gehry, Gehry Partners, Anabelle Selldorf, Selldorf Architects

Cover Design: D/GD (DAKAM Graphic Design)

Print: Metin Copy Plus, Mollafenari Mah., Türkocağı Cad. 3/1, Mahmutpaşa/Istanbul, Turkey

Conference Coordination: DAKAM (Eastern Mediterranean Academic Research Center)

ENTECH '22

VIII. INTERNATIONAL ONLINE ENGINEERING AND TECHNOLOGY CONFERENCE PROCEEDINGS

DAKAM

CONTENTS

QUADCOPTER PLANNING ALGORITHM

ABDALLA AHMED ROSHDI MOHAMED, ÖMER CİHAN KIVANÇ

Abdalla Ahmed Roshdi Mohamed, Engineer, Electrical and Electronics Department of Istanbul Okan University, **Ömer Cihan Kıvanç,** Ph.D., Electrical and Electronics Department of Istanbul Okan University.

Abstract

A quadcopter is one type of several unmanned vehicle systems (UAV), which means it can be operated without a human operator. The environment surrounding the drone can have a lot of obstacles which for sure will create additional difficulties in navigating and planning a path for the drone. The drone will be required to estimate where an obstacle is and it has to manoeuvre accordingly to avoid crashing into it. This mentioned problem requires a very important feature: Obstacle avoidance. The aim here is for the drone to first detect any objects in its surroundings and especially on its path. Then it must avoid hitting it by flying around it or for example flying above it. For this task to be done successfully a lot of complex tasks need to work altogether. A mathematical model should be made for the drone to correctly explain the drone dynamics. This ensures that when the drone is given a new trajectory set of points, they can be translated into some motor voltages that can move the drone to those points accurately. This thesis will mainly compare a widely used planning algorithm with the introduced approach of using the D* lite algorithm. This search algorithm has several advantages over the recent algorithms used for path planning. It can calculate a new path faster while also avoiding newly detected obstacles. Also, the mathematical model, path planning, and path-following algorithms will be explained further in more detail.

INTRODUCTION

It is important to understand the different components and mini-tasks associated with achieving the main target of path planning and path following. As mentioned, the task can be achieved if there is a good mathematical model that can describe the drone dynamics accurately. Also, several sensors will be used to achieve the task and they will be discussed and compared.

QUADCOPTER DESIGN

In a Quadcopter, 4 rotors need to be considered for controlling it. These rotors are placed equidistant from each other. Spinning every two propellers in opposite directions helps in cancelling out the moment caused by the rotation of the propellers. They will help keep the drone stable when they rotate. For that, electronic assistance is required, for example, sensors, controllers, and other electronic components should be used.

QUADCOPTER DYNAMICS

For controlling the drone, some aspects need to be considered first. The frames in which the drone will operate need to be defined for example. The gravity will be pointing in the negative z direction. As can be seen in Figure 1, the x and y are defined in relation to two drone arms. Having the frame defined now it's possible to talk about the different axes in which the drone can rotate. As mentioned before, every 2 propellers rotate in the opposite direction to the other 2 propellers. So, two propellers actually rotate in a specific direction to keep the drone balanced around the x-axis. While the other 2 propellers keep the drone balanced around the y-axis. These 4 propeller rotations in such a way will help in keeping the drone from rotating around its z-axis. Changing the drone's position is related to how fast the motors are spinning. So, a change in their speeds will cause a change in the position as well. To be able to define the drone's position and orientation, 3 axes will be defined as well, namely; the roll, the pitch, and the yaw.

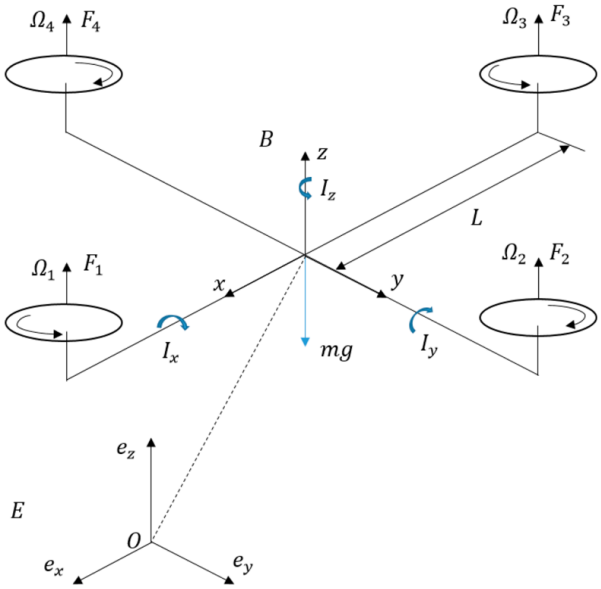

Figure 1. Quadcopter's body frame

QUADCOPTER FORCES AND CONTROL

There are different forces acting on the system. One of the forces is the weight. Then there is the thrust, that's the force caused or generated by the action of the propellers. Another force acting on the drone is the lift (L). An important point to keep in mind here when talking about the lift is the dynamic pressure. Dynamic pressure is the pressure that is caused by the motion of the drone's propellers through the air in this case. The movement and design of the propellers are made in a way so that air moving above the propellers will have lower pressure than air flowing below the propellers. Lower pressure means less force. From that effect, there will be lower pressure above the propeller than below it. This difference in pressure means there will be a net force pointing upwards on the wing producing lift that pushes the propellers upwards.

it is important to know how to define the frames and how to relate them to one another. There is the inertial frame of reference and the body frame of reference. They can be related by introducing a rotation matrix R. If the inertial frame is represented by x, y, and z, while the body frame of reference is represented by a, b, and c. Then they can be related as follows:

$$\vec{a} = R\vec{x};\ \vec{b} = R\vec{y};\ \vec{c} = R\vec{z} \tag{1}$$

where R can be written in relation to the roll, pitch and yaw angles as:

$$R = \begin{matrix} \cos\psi\cos\theta - \sin\phi\sin\psi\sin\theta & -\cos\phi\sin\psi & \cos\psi\sin\theta + \cos\theta\sin\phi\sin\psi \\ \cos\theta\sin\psi + \cos\psi\sin\phi\sin\theta & \cos\phi\cos\psi & \sin\psi\sin\theta - \cos\psi\cos\theta\sin\phi \\ -\cos\phi\sin\theta & \sin\phi & \cos\phi\cos\theta \end{matrix} \tag{2}$$

Calculating the lift force is dependent on three terms: The wing surface area (s), the dynamic pressure (q), and the coefficient of lift (CL). To calculate the dynamic pressure, the equation can be seen below:

$$q = \frac{1}{2} * \rho * V^2 \tag{3}$$

where ρ is the air density, V is the drone speed through the air and it can be measured by the IMU sensors. Then to calculate the lift force (L):

$$L = Cl * q * S \tag{4}$$

The next force to be discussed is the drag force. This force is always acting parallel to the direction of the airflow relative to the vehicle. This means that this force resists the vehicle's motion. Calculating the drag force (D) is dependent on other 3 terms; the drag coefficient, the dynamic pressure, and the surface area of the wing. From these terms, 2 were discussed before. The third term which is the drag coefficient depends on two coefficients; the parasitic drag and another term which contains the coefficient of lift.

$$D = Cd * q * S \tag{5}$$

An important equation that would be used is the equation of moment. It simply says that a moment would cause a rotational acceleration about the axis in which the moment is acting. In the case of 3D representation, the moment will be a vector of length 3 and the rotational acceleration will also be a length 3 vector.

The equation can be seen below:

$$M = I * \dot{w} \tag{6}$$

The term I is the inertial matrix and it will be a 3x3 matrix. In the case of a symmetrical system design the I matrix would look like this form shown below:

$$I = \begin{matrix} I_{xx} & 0 & 0 \\ 0 & I_{yy} & 0 \\ 0 & 0 & I_{zz} \end{matrix} \tag{7}$$

This equation is valid and works only when dealing in the world frame. However, all the moments and accelerations are defined in the body frame. Even the gyroscopes measurements are relative to the body frames. This means that this equation alone can't be used and more complex mathematical terms need to be added. The equation after adding the terms will look like this:

$$M = (I * \dot{w}) + w \times (Iw) \tag{8}$$

Using the moment equation in x, y, and z directions it is possible now to calculate omega dot, from which it is possible to calculate and update 9 of the 12 states by doing simple integrations. The only terms left is ϕ, θ and Ψ. To calculate them a rotation matrix will be needed for that. This rotation matrix will define how to transform from the world frame to the body frame. The equation can be seen below:

$$\begin{matrix}\dot{\phi} \\ \dot{\theta} = \\ \dot{\psi}\end{matrix} \begin{matrix}1 & \sin(\phi)\tan(\theta) & \cos(\phi)\tan(\theta) \\ 0 & \cos(\phi) & -\sin(\phi) \\ 0 & \sin(\phi)/\cos(\theta) & \cos(\phi)/\cos(\theta)\end{matrix} * \begin{matrix}p \\ q \\ r\end{matrix} \quad (9)$$

The 3x3 matrix in the middle is the rotation matrix that transforms the Euler angles in the body frames to the angular velocities in the world frames. The controllers used for this drone will mainly be PID controllers. There are 3 parts in the system that needs to be controlled. The altitude, the lateral position, and the yaw angle. The z trajectory will be handled by the altitude controller. The altitude controller's goal is to set the collective thrust to reach the required altitude. Then there are the x and y trajectories, they will first be handled by the level position controller. The yaw trajectory will be handled by the yaw controller. The altitude controller is fed by the reference z and the measured and estimated z. The output from the altitude controller will be fed also to the roll-pitch controller. That is because the thrust also can affect not only the z position but also the x and y positions of the drone. The other inputs to the roll-pitch controller come from the lateral controller. The outputs from the roll-pitch controller are the required roll and pitch rates. These outputs will be fed to the body rate controller. This is a simple P controller that converts p, q, and r commands into 3 rotational moment commands. The r command is received from the yaw controller. The altitude controller is a PD controller. The yaw, roll-pitch, and body rate controllers are all of the first order. Thus, they are designed as just P controllers.

SENSORS FOR NAVIGATION

The task of navigation is what will keep the drone flying. It is simply what makes the drone fly from one point to another. The sensors used for this task are IMU and GPS sensors. Information from these sensors is used by the computer as inputs and the computer will apply sensor fusion using an Extended Kalman Filter (EKF) and then convert this information into thrust values. These values are then sent to the Electronic Speed Controller (ESC), which has a PID controller, to apply the required voltages to the motors which in turn will apply the required forces to make the drone move as needed.

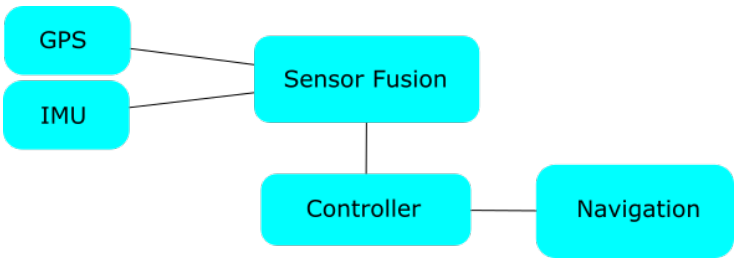

Figure 2. Navigation task

SIMULATOR

The simulator used is one made by Udacity using Unity (Domluna, Available 2018). The simulator includes two different parts. One for free flying and to try different lines of code. The other one is for motion planning

of the drone and trying different planning algorithms. Using this simulator, python code will be written to control the drone in the simulation. This same code, after testing it in the simulations, can be used on a real quadcopter and can be uploaded to a flight computer.

PLANNING

The motion planning problem is the main focus of this project. Planning here is answering the question of how the drone should reach the goal it is required to reach in the most efficient way possible without hitting or crashing into any obstacles (Aye Aye Maw, M. T. a. J.-W. L., 2018). This planning problem is just a step and is actually something computed by the flight computer. So, the planning problem output will be a set of trajectories that the drone should follow to reach its goal. The motion planning state machine can be shown in Figure 3. This diagram shows the many tasks a drone should do in order to have a successful flight. It can be seen that the planning task is just one step in this diagram.

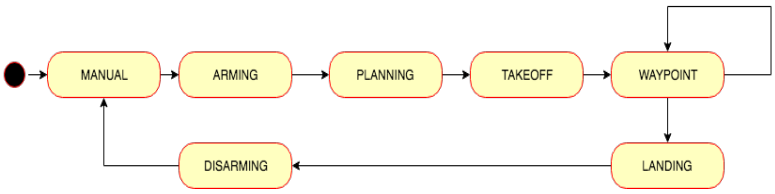

Figure 3. Motion planning state machine

The world can be represented as a grid or a group of squares. This planning method is known as Graph Search Method in which the workspace is divided into cells and then the cells are connected as a graph or a roadmap. After deciding on the design of the grid, now it's important to assign a cost to the actions that can be done by the drone. This cost can be used then to compare different plans (Hart, P. (1968)). The cost can be taken as the Euclidean metric distance from the starting to goal point. This can be shown as follows:

$$Cost = \sum_{n=1}^{n-1} \sqrt{(x_{n+1} - x_n)^2 + (y_{n+1} - y_n)^2} \tag{10}$$

where the summation is for the cost of traveling between nodes to move from the starting point to the current point. Another important aspect that needs to be taken into mind is what's called heuristics (Pearl, J. 1985). Given the map of the world and the grid, now an estimate of how far the distance any given square on the grid to the goal can be calculated. Now, by using the cost function and the heuristics the planning problem can be solved.

A* and D* Lite Algorithms

For planning a path in an environment that is well-known and static, the A* algorithm would achieve greatly (Likhachev, M. a. K. S., 2001). But this is not always the case. It is almost always that the environment is dynamic, obstacles show up in the drone's path and these obstacles are not taken into account. In this case, the A* algorithm would be computationally complex and costly (Koenig, S., and Likhachev, M. 2001). The problem is that every time an obstacle is detected, the A* algorithm has to be run again to find a new path while avoiding the obstacle. The D* lite algorithm is an adaptation of the A* algorithm but in addition, it

incorporates incremental search (Stentz, A. (1995)). This means that the algorithm will reuse the information that was calculated from the previous searches instead of solving each search again from scratch. That makes the D* lite a better algorithm for solving this replanning issue when detecting an obstacle (Koenig, S. and Likhachev, M. (2002)). This algorithm, in contrast to the A* algorithm, runs from the goal point to the starting point. This is the main difference between both algorithms. The advantage here is that if the starting point changes, the existing tree paths can be used to quickly find a new path from the end node to the start node. Also with this advantage, the D* lite algorithm was shown to give better results when used as the planning algorithm in case of flying the drone in an unknown environment. So, if the map was not already given as data and instead the drone has to figure out on its own the environment around it and find the best path to reach the goal, the D* lite would be the better algorithm to use in such a situation. Now considering an example where the drone is flying in unknown terrain and it was given a goal point where it should fly to. The drone should observe which adjacent cells are free and traversable and then it should move to one of them. From its starting position, the drone has to reach its goal. While doing that, the drone should compute always the shortest distance or else, the path with the lowest cost. The cells which have not been explored yet are taken as traversable, meaning that they can be included in the planned path of the drone. The drone will follow the planned path until it reaches its goal or until it explores a cell with an obstacle. If a cell with an obstacle was explored, the drone should recompute a new path from its new current position.

```python
def scanForObstacles(graph, queue, s_current, scan_range, k_m):
    states_to_update = {}
    range_checked = 0
    if scan_range >= 1:
        for neighbor in graph.graph[s_current].children:
            neighbor_coords = stateNameToCoords(neighbor)
            states_to_update[neighbor] = graph.cells[neighbor_coords[1]
                                                     ][neighbor_coords[0]]
        range_checked = 1
    # print(states_to_update)

    while range_checked < scan_range:
        new_set = {}
        for state in states_to_update:
            new_set[state] = states_to_update[state]
            for neighbor in graph.graph[state].children:
                if neighbor not in new_set:
                    neighbor_coords = stateNameToCoords(neighbor)
                    new_set[neighbor] = graph.cells[neighbor_coords[1]
                                                    ][neighbor_coords[0]]
        range_checked += 1
        states_to_update = new_set

    new_obstacle = False
    for state in states_to_update:
        if states_to_update[state] < 0:  # found cell with obstacle
            # print('found obstacle in ', state)
            for neighbor in graph.graph[state].children:
                # first time to observe this obstacle where one wasn't before
                if(graph.graph[state].children[neighbor] != float('inf')):
                    neighbor_coords = stateNameToCoords(state)
                    graph.cells[neighbor_coords[1]][neighbor_coords[0]] = -2
                    graph.graph[neighbor].children[state] = float('inf')
                    graph.graph[state].children[neighbor] = float('inf')
                    updateVertex(graph, queue, state, s_current, k_m)
                    new_obstacle = True
        # elif states_to_update[state] == 0: #cell without obstacle
            # for neighbor in graph.graph[state].children:
                # if(graph.graph[state].children[neighbor] != float('inf')):

    # print(graph)
    return new_obstacle
```

```python
def moveAndRescan(graph, queue, s_current, scan_range, k_m):
    if(s_current == graph.goal):
        return 'goal', k_m
    else:
        s_last = s_current
        s_new = nextInShortestPath(graph, s_current)
        new_coords = stateNameToCoords(s_new)

        if(graph.cells[new_coords[1]][new_coords[0]] == -1):  # just ran into new obstacle
            s_new = s_current  # need to hold tight and scan/replan first

        results = scanForObstacles(graph, queue, s_new, scan_range, k_m)
        # print(graph)
        k_m += heuristic_from_s(graph, s_last, s_new)
        computeShortestPath(graph, queue, s_current, k_m)

        return s_new, k_m
```

Figure 4. Code for detection of obstacles

As a code, the D* lite algorithm would not differ too much from the A* algorithm. As discussed before the main difference would be that the search will start from the goal node to the starting node. Then some functions will be added which are related to detecting obstacles and how the algorithm should deal with them. The function shown in Figure 4 is related to checking if an obstacle is detected in the neighbourhood of the current node. If there is an obstacle detected it will just return a "True", while if there are no obstacles detected, the returned value will be "False".

The value returned from the scanForObstacles() function will be used in this other function called moveAndRescan(). As the name suggests, this function will move a step and check if there are any obstacles in the neighbouring nodes. As discussed before, the neighbouring nodes with obstacles will be assigned a cost of infinity and will not be included in the next path that will be planned.

SIMPLIFYING THE PATH

When planning the path, and after finding a feasible path to reach the goal, the drone is required to follow a number of waypoints to reach the goal point. By designing the world in a grid shape, each grid will be a waypoint for the drone. This means that each square on the grid on the calculated path is a temporary goal for the flight computer. The problem with this is that the drone will stop at each waypoint. This is not a good way to achieve the goal. Instead, it would be better to find a way to shorten the unnecessary waypoint in between. A method is needed to know the points on the same line. For this, a mathematical rule can be used, which is collinearity. This rule implies that if the area inside any three points is zero, then they are on the same line. This can be applied to each triplet of points on the path. For every three points that are proved to be collinear, the middle point can then be removed.

Another important point that can lower the number of waypoints, and it can achieve a more optimal path is to find the diagonal paths instead of moving right and then up for example. This can be done by a method called Ray Tracing but it has a disadvantage, it's so computationally expensive since the numbers dealt with can be possibly float values. A solution for this is to use the Bresenham method, which is a way that achieves the same task but deals with integer values instead of dealing with float values.

DEADBANDS

Now, the next step is to ensure the plan will be executed smoothly. For this to happen, the drone shouldn't stop at each waypoint, instead, it must move from a waypoint to the other continuously. The problem here is that the position of the drone is mostly received by a GPS signal which can be affected by a lot of things like the quality of the components or even atmospheric changes. For the drone, this will look like the path itself is moving around. This will cause the flight controller to send a lot of different signals that will affect the smoothness of the flight. To solve this issue, the idea of a dead band can be introduced to the flight controller. A dead band is simply an area that will be around the waypoints. When the drone reaches this area of the first waypoint, the flight controller will start to give the drone commands to go to the next waypoint instead of trying to reach exactly the first waypoint.

KALMAN FILTER FOR SENSOR FUSION

The measurements from the sensors were merged to achieve more accurate results. For merging EKF was used. A Kalman filter is an optimal estimator which is used to predict measurements from inaccurate and uncertain measurements (Ribeiro, M.I., 2004). Kalman filters are widely used because of their online real-time processing and the simplicity of formulation as well as their optimality. The basic Kalman filter cannot be used to solve nonlinear problems because it is based on the assumption that the motion and measurement models can be in the Gaussian world. This is not the case when dealing with nonlinear functions. The linearization method makes use of the Taylor approximation. A jacobian matrix will be used

to linearize the prediction and the correction parts. The prediction contains two parts: prediction of the state and prediction of the covariance matrix of the noise. These can be written as the following:

$$\bar{\mu_t} = g(u_t, \mu_{t-1}) \tag{11}$$

$$\bar{\Sigma_t} = G_t \Sigma_{t-1} G_t^T + R_t \tag{12}$$

The next step is to correct these estimations. The correction part occurs based on the measurement units which are the sensors. In the drone case, the measurement is got from the GPS and the IMU sensors. The correction part also includes an important weighting factor which shows how much the measurements from the sensors can be trusted over the prediction. For example, when the drone is in a tunnel, the GPS signal cannot be trusted much because GPS needs to be in light of sight with the satellites. In this case, IMU sensor can be trusted more as well as the prediction calculated from using the system model. The correction part can be written as follows:

$$K_t = \bar{\Sigma_t} H_t^T (H_t \bar{\Sigma_t} H_t^T + Q_t)^{-1} \tag{13}$$

$$\mu_t = \bar{\mu_t} + K_t(z_t - h(\bar{\mu_t})) \tag{14}$$

$$\Sigma_t = (I - K_t H_t)\bar{\Sigma_t} \tag{15}$$

The H_t and G_t are the jacobian matrices linearizing the function at specified μ_t. The K_t matrix shows how much the measurement can be trusted over the prediction.

FINAL SIMULATION RESULTS

The simulation will be started with the quadrotor at a random rest point in the map. Then a final goal point will be given that the drone should reach. The diagram below shows the drone at rest and the environment surrounding it. The latitude, longitude and altitude information can be seen on the top left part.

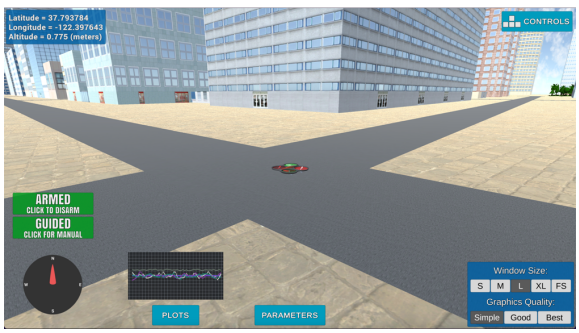

Figure 5. Drone and its environment

The computation of the trajectory takes a little time, around 85 seconds, based on how far the initial and final positions are from each other and based on the number of obstacles in the way. The algorithm is trying to find the best optimal path as discussed before. For both discussed algorithms, A* and D* lite, the first run for a given known map will take almost the same time to find a path, however, this simulation was run with the D* lite algorithm.

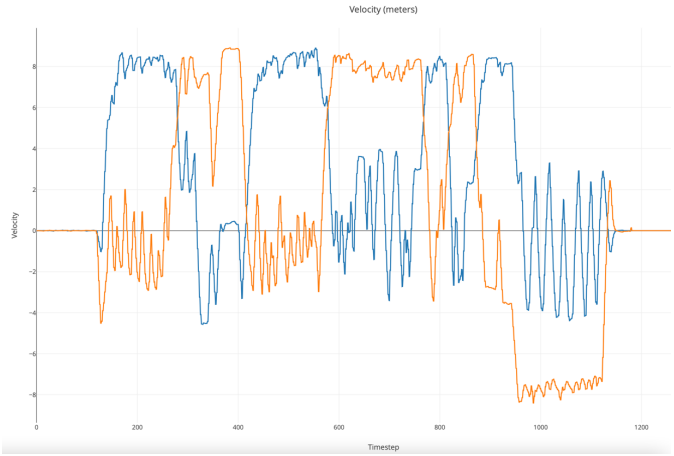

Figure 6. Velocity in roll and pitch

The altitude graph shown in Figure 7 shows an increase in the amplitude at the middle of the flight time. This increase resulted because there was a short building that the drone can fly above it while keeping the cost low. Other buildings are too tall in the simulation and it would increase the cost if the drone planned a path from above them. Figure 8 shows the path the drone took to reach its goal position.

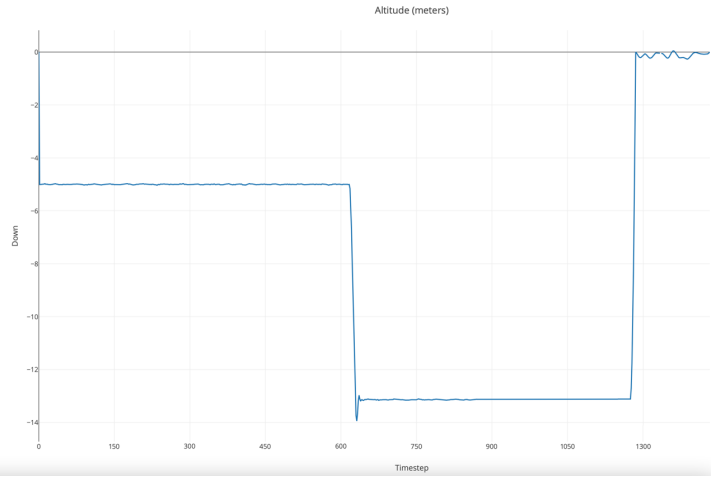

Figure 7. Altitude of the drone

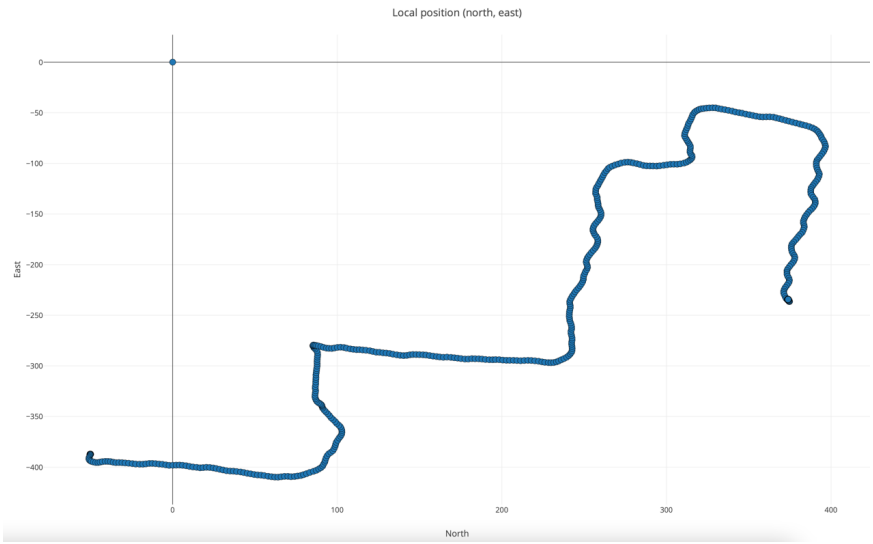

Figure 8. Position of the drone

Now, the error between the target point and the real position of the drone will be compared. It is important to remember the concept of dead band discussed before. This will cause the error between the target and the real value to be slightly higher than zero because the dead band allows the drone to reach an area around the target point and not exactly on it. The error reaches a minimum value of 1.44 as can be seen in Figure 9. The only point the error gets very low is at the final point. The error reaches a value of 0.2 meters which is not high taking into consideration GPS and IMU uncertainties. The reason why the error reaches the lowest value at the final position is that there is no dead band introduced at the end position. It is assumed that the drone must reach the final point exactly and that it is critical. So, no dead band is added at the final position. It can be seen that from time 20 until time 40, the drone was hovering in place, this can be seen from the error that it was not increasing or decreasing. This occurs for the fact that there are some buildings that were removed from the map file that is fed to the algorithm. So, they will be added during the simulation to be dealt with as discovered obstacles on the way. So, the time taken by the D* lite algorithm to find a new path was around 20 seconds.

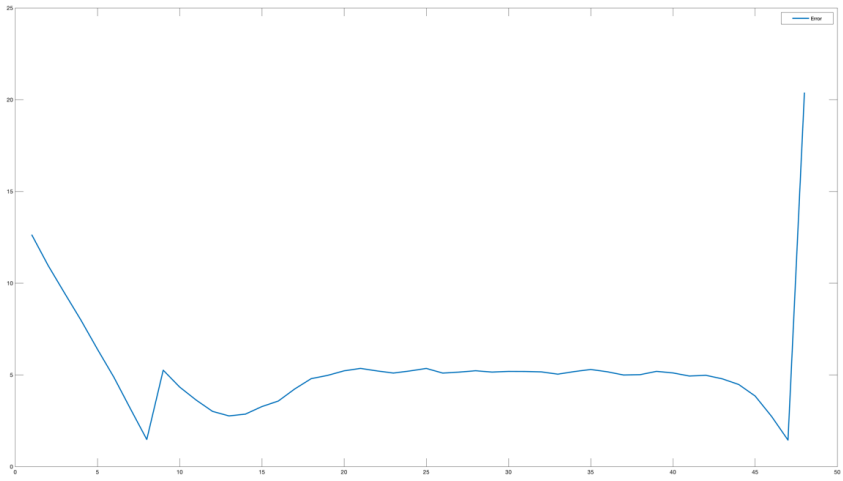

Figure 9. Error between target and real drone's position using D lite*

The same is applied now using the A* algorithm to see how long it will take to find a new path after discovering the new obstacles. Figure 10 shows the error again between the target point and the real drone's position while using the A* algorithm for path planning. It can be seen that the drone hovered in place for around 180 seconds this time. This shows how fast the D* lite algorithm is compared to the A* algorithm when used in a changing environment. This simulation was repeated several times while changing the number of obstacles added during the flight.

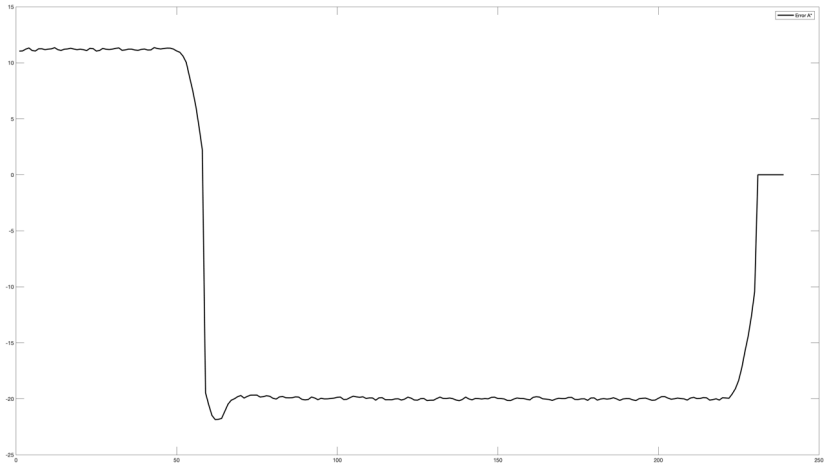

*Figure 10. Error between target and real drone's position using A**

As can be seen from Figure 11, for both algorithms the number of node expansions increased linearly with the number of obstacles discovered. However, the rate of increase with the A* algorithm shows double the increase of the D* lite algorithm. The result for the number of node allocations shows almost a constant value for the D* lite algorithm, while there was again a linear increase for the A* algorithm. These results show that the D* lite algorithm works better and faster than the A* algorithm when dealing with an unknown environment which is exactly the case with the drone.

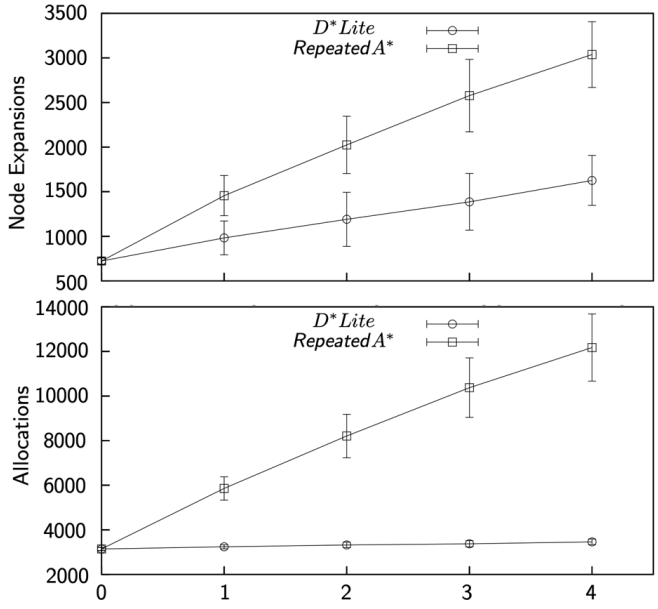

Figure 11. Effect of obstacles discovered on A and D* lite (Mackay, D., 2005)*

CONCLUSION

In this project, a drone simulation was used. Different aspects were looked at including the sensors used and why they were selected. Then the dynamics and control aspects were also discussed. After that the main focus of the project, which is solving the path planning problem, was examined and looked at. It was seen how the two algorithms, the A* and the D* lite, are different. The main difference between these algorithms is that the D* lite algorithm searches from the goal node toward the starting node, while the A* algorithm goes the other way. The D* lite algorithm was seen to perform better, especially in the case where the environment is unknown. Even when the environment is known but there are obstacles that can show up in the environment, the D* lite algorithm would achieve better results.

REFERENCES

- Koenig, S. and Likhachev, M., 2001. Incremental a. Advances in neural information processing systems, 14.

- Koenig, S. and Likhachev, M., 2002, May. Improved fast replanning for robot navigation in unknown terrain. In Proceedings 2002 IEEE international conference on robotics and automation (Cat. No. 02CH37292) (Vol. 1, pp. 968-975). IEEE.

- Stentz, A., 1995, August. The focussed d^* algorithm for real-time replanning. In IJCAI (Vol. 95, pp. 1652-1659).

- Hart, P.E., Nilsson, N.J. and Raphael, B., 1968. A formal basis for the heuristic determination of minimum cost paths. IEEE transactions on Systems Science and Cybernetics, 4(2), pp.100-107.

- Pearl, J., 1984. Heuristics: intelligent search strategies for computer problem solving. Addison-Wesley Longman Publishing Co., Inc..

- domluna, Available 2018. FCND Simulator. [Online] at: https://github.com/udacity/FCND-Simulator-Releases/releases/tag/v0.1.0-motion-planning

- Likhachev, M. a. K. S., 2001. Lifelong Planning A*and Dynamic A* Lite. The proofs. Technical report, College of Computing, Georgia Institute of Technology,Atlanta.

- Maw, A.A., Tyan, M. and Lee, J.W., 2019. Development of Flight Mission Planner using Intelligent Anytime Planning and Replanning Algorithm for UAV Operation (Doctoral dissertation, MERAL Portal).

- Ribeiro, M.I., 2004. Kalman and extended kalman filters: Concept, derivation and properties. Institute for Systems and Robotics, 43, p.46.

- Mackay, D., 2005. Path planning with d*-lite. DRDC Suffield TM, 242.

THERMOHYDRAULIC ANALYSIS OF JET IMPINGEMENT COOLING OPERATING WITH A POROUS LAYER AND HYBRID NANOFLUIDS

ZAKARIA KOREI*, SMAIL BENISSAAD

Applied Energetics and Pollution Laboratory, Department of Mechanical Engineering, Faculty of Sciences Technology, University of Mentouri Brothers -Constantine 1, Algeria.

ABSTRACT

This investigation aims at performing a numerical analysis of jet impingement cooling on a hot plate operating with a porous layer and silver-magnesium oxide/water (Ag-MgO/H2O) hybrid nanofluid as a working fluid using the Finite Volume Method (FVM). Parameter's analysis is provided under forced convection conditions by varying Reynolds number, solid volume fraction, and porosity. The outcomes are given in terms of average Nusselt number and pressure drop. The results show that decreasing porosity leads to an increase in heat transfer and pressure drop. In addition, the suspensions of nanoparticles in the base fluid increase the average Nusselt number and pumping power.

Keywords . Heat transfer. Forced convection. Porous layer. Nanofluids. Jet impingement. Cooling.

1.INTRODUCTION:

Impinging jets are used in modern industrial equipment to cool, heat, or dry surfaces in specific areas. Creating high localized heat transmission is the main benefit of impinging jets [1]. The methods to obtain high-performance cooling can be achieved by operating the system with a porous medium or using a nanofluid as the working fluid.

Various experimental and numerical studies on the usefulness of nanofluids and porous media in different fields are available in the literature. For example, Hassan et al. [2] investigated ways to improve heat transfer using nanofluids expelled from a slot jet and impinging on a flat surface. Their results show a significant increase in the average Nusselt number as the solid volume fraction increased. Zeitoun et al. [3] investigated experimentally the heat transmission properties between a circular nanofluid jet and a horizontally heated disk. Their experimental data demonstrate an increase in the Nusselt numbers as the nanoparticle concentration. SiO2-water nanofluids were applied to impinging jets by Lv et al. [4]. They proposed correlations for heat transmission between a vertical circular free surface jet of SiO2-water nanofluids and a horizontal circular plate.

Chinige et al. [5] utilized the Lattice Boltzmann method to study the convective heat exchange properties of impinging jets in the presence of a porous substance. According to numerical research, decreasing the Darcy number will increase the stagnation of Nu. In order to examine the impact of adding periodic vertical porous and solid ribs with varied geometrical forms, Lori and Vafai [6] conducted a thorough computational assessment of fluid flow and heat transfer in a 3D micro-channel. It was found that decreasing Darcy number and porosity increases pressure drop.

As mentioned above, the importance of nanofluid and porous media on heat transmission. The objective of this report is to study the hybrid impact of the porous layer and hybrid nanofluids in the jet impact cooling problem. The effects of the Reynolds number, the volume fraction of the hybrid nanofluid, and the porosity are studied.

2.PROBLEM FORMULATION:

The problem is illustrated in Figure 1, having a single circular jet of diameter (w) and the height between the jet and the target plate (H). A uniform velocity and temperature are defined in the inlet conditions. The pressure outlet condition was used at the outlet. A constant heat flux is used for the target wall, and the other walls are adiabatic.

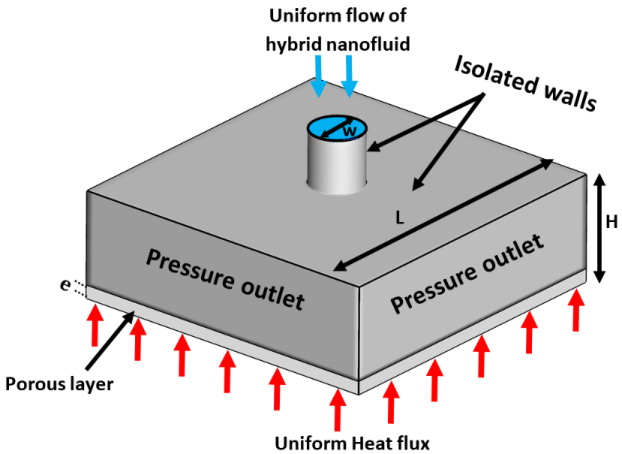

Figure 1. Computation domain.

3.MATHEMATICAL FORMULATIONS

The hybrid nanofluid flow is regarded to be Newtonian, three-dimensional, steady, and incompressible. The Brinkman Darcy–Forchheimer equations are used to account the effects of porous media.

The governing equations based on the previous hypotheses are :

Continuity equation:

$$\nabla.\left(\rho_{hnf}V\right) = 0 \tag{1}$$

Momentum equation:

$$\frac{\rho_{hnf}}{\varepsilon^2}\nabla.(VV) = -\nabla P + \frac{\mu_{hnf}}{\varepsilon}\nabla^2 V - \frac{\mu_{hnf}}{K}V - \frac{F_c}{\sqrt{K}}V|V| \tag{2}$$

Energy equation:

$$\left(\rho C_p\right)_{eff}\nabla.(T) = k_{eff}\nabla^2 T \tag{3}$$

And the equation for heat transfer by conduction is:

$$k_s\nabla^2 T_s = 0 \tag{4}$$

The effective specific heat and thermal conductivity of the porous domain are calculated as follows:

$$k_{eff} = (1-\varepsilon)k_s + \varepsilon k_{hnf} \tag{5}$$

4.NUMERICAL METHOD AND CODE VALIDATION

The computational domain was established in ANSYS Design 14.5, and the meshing was performed in ANSYS Meshing 14.5 (Figure 2). The Ansys fluent 14.5 solver was used to solve the governing equations. The pressure-velocity coupling is generated using the SIMPLE approach. Using a second-order technique, the convective terms in the equations are discretized.

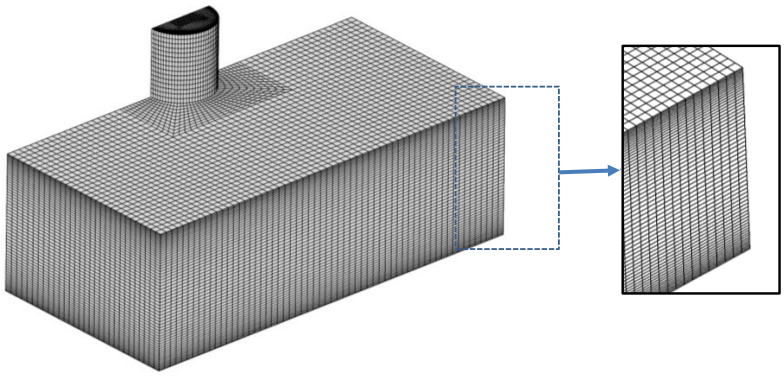

Figure 2: Grid distribution

The grid independence research is conducted with four different grids to ensure that the results are independent of the size of the grid.

The numerical code was validated by comparing our numerical results with previously published data [7] (Figure 3).

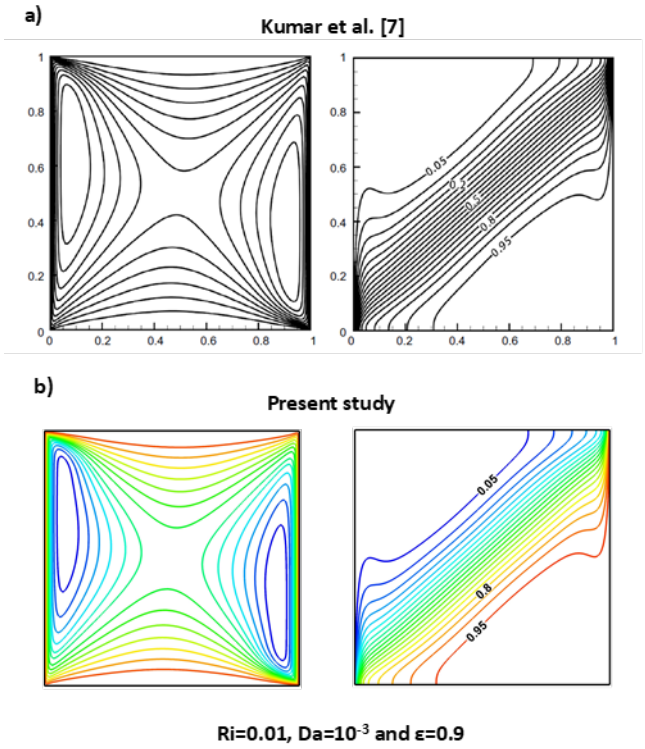

Figure 3: comparison of streamline and isotherm with a previously published study [7]

5.RESULT AND DISCUSSION

In this section, we present the effect of different parameters: Reynolds number, volume fraction, and porosity on isotherms, average Nusselt number, and pressure drop.

5.1.Average Nusselt number

The impact of porosities and Reynolds number on the heat transfer rate is given in Figure 4. As can be seen, the average Nusselt number increases as the Reynolds number increases and porosity decreases. This is mainly related to the increase in the mechanism of convection and conduction. Moreover, it can be observed that the effect of porosities is more pronounced at higher Reynolds numbers.

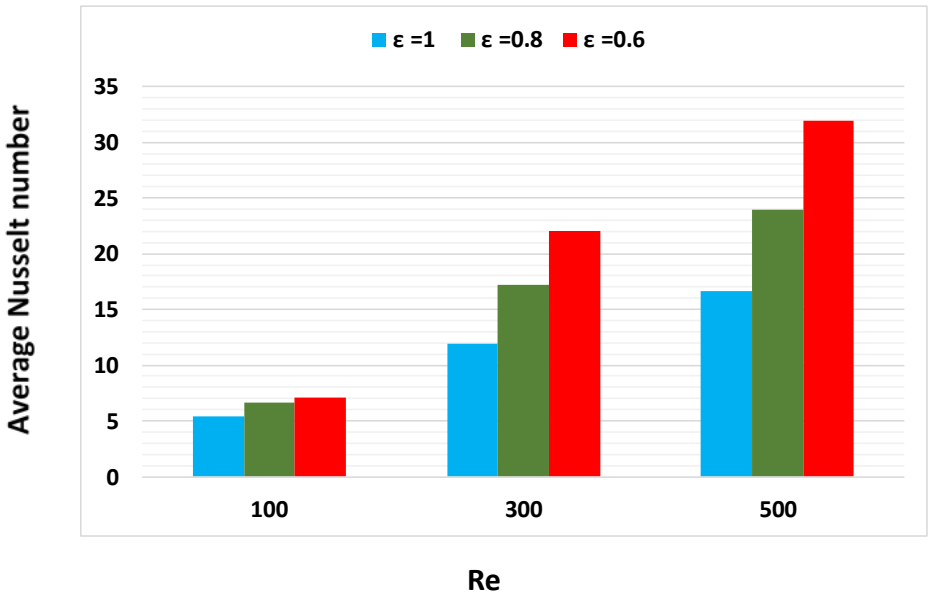

Figure 4. Average Nusselt number as a function of Reynolds number for different porosities.

Figure 5 shows the average Nusselt number as a function of solid volume fraction for different Reynolds numbers. The figure illustrated that the suspension of nanoparticles in the base fluid increases the thermal transmission, whatever the value of the Reynolds number, which can be explained by the increase in the effective thermal conductivity.

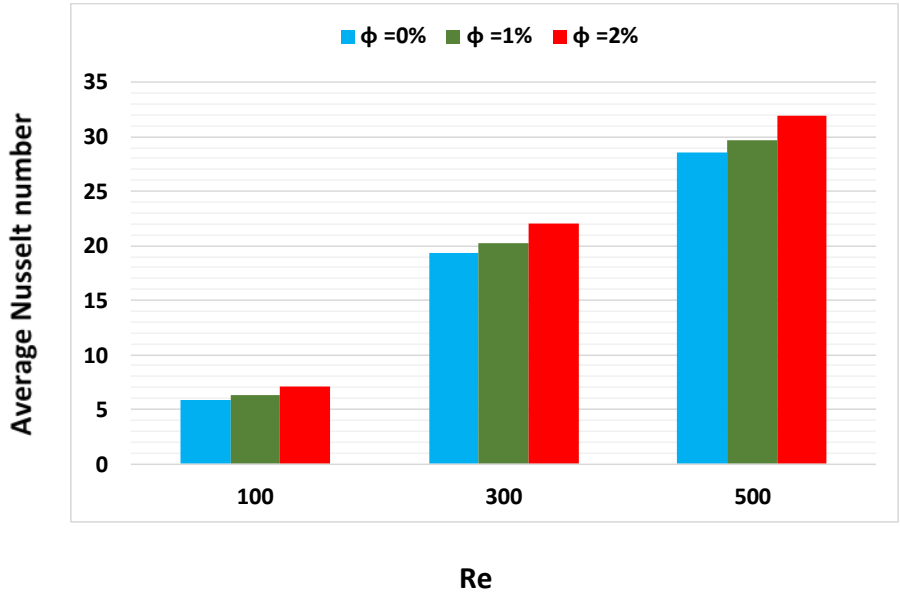

Figure 5. Average Nusselt number as a function of Reynolds number for different solid volume fractions.

5.2.Pressure drop

Figure 6 shows the effect of porosities and Reynolds number on pressure drop. It can be observed that the pressure drop increases as the inlet velocity increases, as expected due to the increase in friction. However, a slight increase in pressure drop when operating the system with a porous layer.

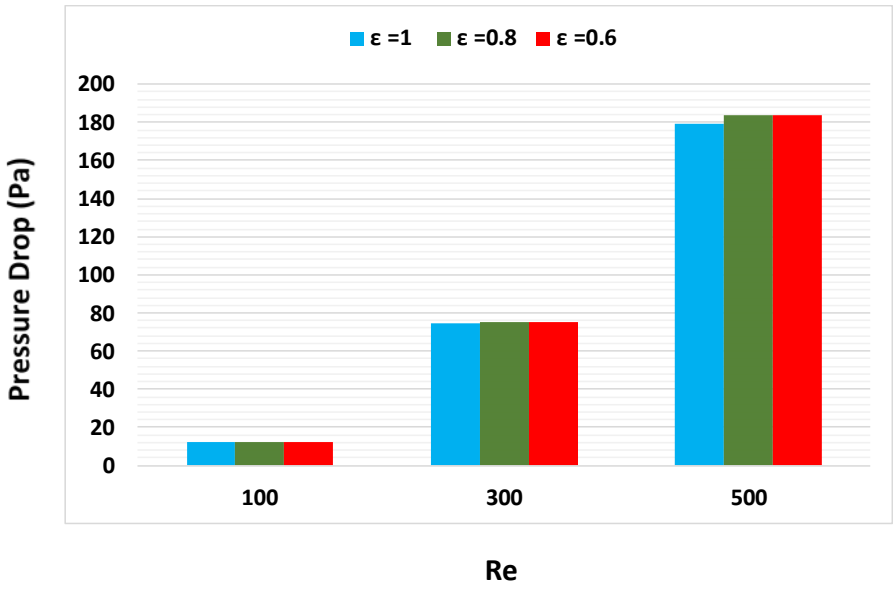

Figure 6. Pressure drop as a function of Reynolds number for different porosities.

Finally, the effect of increasing the solid volume fraction on the pressure drop is shown in Figure 7. As seen in the figure, the pressure drop increases as the solid volume fraction increases due to an increase in effective dynamicviscosity, which increases friction.

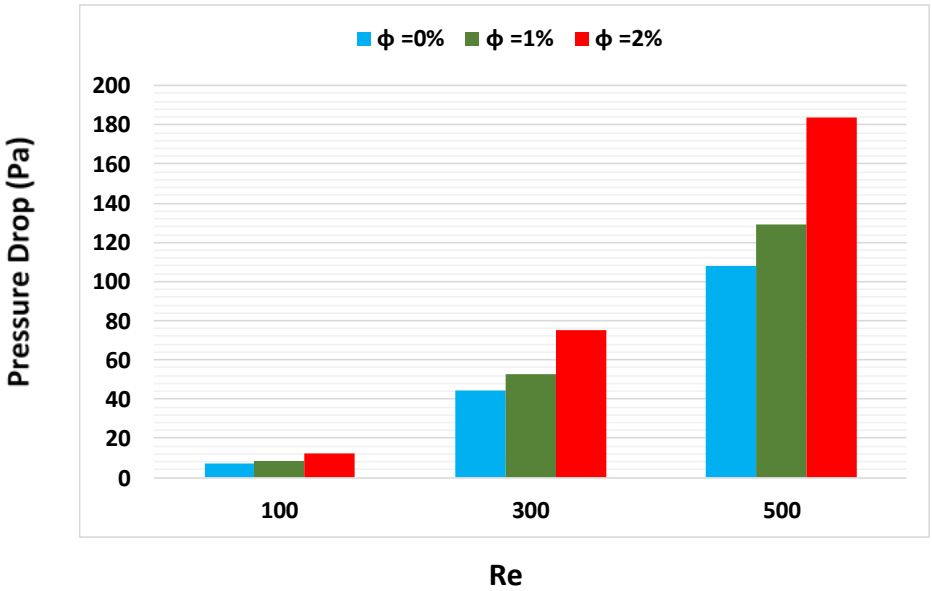

Figure 7. Pressure drop as a function of Reynolds number for different solid volume fractions.

6.CONCLUSIONS

Thermohydraulic analysis in a cooling problem by jet impingement operating with Ag-MgO/H2O hybrid nanofluid and a porous layer is studied numerically. The finite volume method was used to solve governing equations. The obtained results allowed us to observe that heat transfer and pressure drop increased when porosity was reduced. Also, the average Nusselt number and pumping power rise when nanoparticles are suspended in the base fluid.

REFERENCES

[1] F.T. Dórea, M.J.S. de Lemos, Simulation of laminar impinging jet on a porous medium with a thermal non-equilibrium model, International Journal of Heat and Mass Transfer. 53 (2010) 5089–5101. doi:10.1016/j.ijheatmasstransfer.2010.07.055.

[2] M.M. Hassan, M.A. Teamah, W.M. El-Maghlany, Numerical investigation for heat transfer enhancement using nanofluids over ribbed confined one-end closed flat-plate, Alexandria Engineering Journal. 56 (2017) 333–343. doi:10.1016/j.aej.2017.03.051.

[3] O. Zeitoun, M. Ali, Nanofluid impingement jet heat transfer, Nanoscale Research Letters. 7 (2012). doi:10.1186/1556-276x-7-139.

[4] J. Lv, C. Hu, M. Bai, K. Zeng, S. Chang, D. Gao, Experimental investigation of free single jet impingement using SIO 2 -water nanofluid, Experimental Thermal and Fluid Science. 84 (2017) 39–46. doi:10.1016/j.expthermflusci.2017.01.010.

[5] C.S. Kumar, S. Mohankumar, M. Geier, A. Pattamatta, Numerical investigations on convective heat transfer enhancement in jet impingement due to the presence of porous media using cascaded lattice Boltzmann method, International Journal of Thermal Sciences. 122 (2017) 201–217. doi:10.1016/j.ijthermalsci.2017.08.020.

[6] M.S. Lori, K. Vafai, Heat transfer and fluid flow analysis of microchannel heat sinks with periodic vertical porous ribs, Applied Thermal Engineering. 205 (2022) 118059. doi:10.1016/j.applthermaleng.2022.118059.

[7] Kumar, D. S., Dass, A. K., & Dewan, A. (2009). Analysis of Non-Darcy models for mixed convection in a porous cavity using a multigrid approach. Numerical Heat Transfer, Part A: Applications, 56(8), 685–708. https://doi.org/10.1080/10407780903424674.

LAND USE CLASSIFICATION DATASET FOR SHKUMBINI WEAP MODEL, APPLYING QGIS SOFTWARE

LILJANA LATA

P.h.D Student, Institute of GeoSciences, Energy, Water and Environment (IGEWE), Polytechnic University of Tirana, Albania

Abstract

Shkumbini river basin, as one of the seven biggest river basins in Albania, requires a proper management plan. Assessment of pressures on surface water and groundwater and their influence over water resources and environment should necessarily be considered. Different uncontrolled developments that have taken place primarily in the lowlands of the river basin have been a contributing factor to the rapid intensification of the erosion process, reducing green corridors and compromising environmental balances. Furthermore, data on natural conditions in conjunction with background statistic evaluations, including land use and land cover (agriculture, forestry, roads, constructed environments, etc.) have been crucial aspects during the first attempt of building a Water Evaluation and Planning (WEAP) model for the Shkumbini river. On this basis a reliable assessment of the water body status requires an appropriate knowledge of the whole hydrological conditions that continuously change, seasonally and annually. Additionally, the assessment helps to identify and analyze essential water system vulnerabilities with regard to future climate change and development scenarios.

INTRODUCTION

This document represents a detailed description of the methodology and calculations used for the assessment of the Land Cover areas for Shkumbini WEAP model. This effort is a part of the work in process for implementing an integrated water resource management model via utilization of WEAP (Water Evaluation and Planning) system, developed by SEI (Stockholm Environmental Institute). Land cover data was originally obtained from the EU CORINE 2012 dataset, covering the calibration period of the model (1991-2016). The WEAP model development was impelemented utilizing the open source QGIS software. The watershed elements in the WEAP model allow us to calculate the areas of different land use types within a catchment and specify their corresponding hydrology through calibration process. The model works on the principle that various land use areas can generate specific run-off, although only certain land use types permit that the intensive rainfall becomes instantaneous streamflow. Other areas may retain water and release it gradually, producing a constant run-off especially during periods of low rainfall. Once the values associated with land use parameters have been obtained and organized, future scenarios can explore the outcomes of land use changes. Finally, following the WEAP format requirements (SEI, 2016), a range of other specific methodologies were applied during the dataset preparation process.

Study area: Shkumbini River basin is completely situated within Albanian territory, located in its middle part (see Figure 1). Its basin, encompassing an area about 2464 km^2 is surrounded by mountain ranges from east to west generally, higher than 1500 m above sea level such as Valamara (2375 m), Kamje (1625 m) in the west, and Shebenik (2,180 m) and the Mokra mountains (2,148 m) in the easter part. Originating from these mountains, Shkumbini river is classified as a typical mountainous river, flowing in a relatively steep slope especially for the upstream part until reaching the city of Elbasan. The mean altitude of the river basin is around 753 m above sea level. Before flowing into the Adriatic Sea, Shkumbini River absorbs the waters of its biggest tributaries such as Bushtrica, Hotoloshti, Rrapuni, Gostima, Zaranika and Kusha. The annual average discharge of the river is about 58 m^3/s. Various small glacial lakes and reservoirs are present, especially in the upper section of the river basin. The Shkumbini River intersects 5 important prefectures along its 181,4 km length: Tiranë (the capital of Albania), Elbasan, Fier, Korçë, and Dibër. It runs with meanders through a narrow river bed before entering the Adriatic Sea by the Karavasta Lagoon. Shkumbini River Basin has a total population of around 413.293 inhabitants, mostly living in western flat areas of the basin, where urban areas with the biggest population density of the basin such as Elbasani city are situated; population density for Elbasani city goes up to 3567 inhabitants/km^2, and that of Kavaja city up to 2549 inhabitants/km^2.

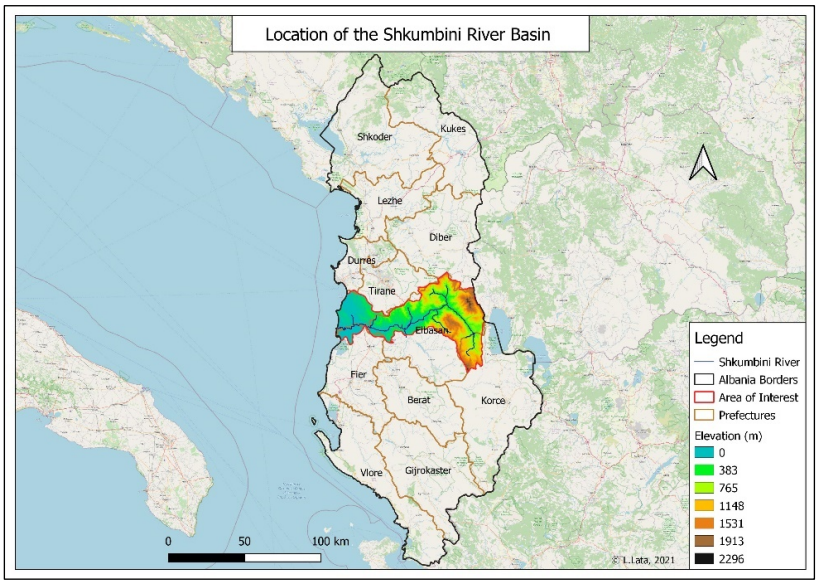

Figure 1. The Shkumbini river basin location; source: own elaboration.

The climate is typical Mediterranean, characterized by hot and dry summers and wet and mild winters. The mean annual precipitation in the catchment is 1400 mm. The snow is a normal phenomenon during the winter, especially on the eastern part of the river basin. Around half of the river basin has ultrabasic formations and the other half has calcareous and terrigenous formations, making it possible for this river basin to be rich in karst groundwater aquifers and water sources, thus providing good quality water to the above-mentioned urban areas. The groundwater availability is typically influenced by various factors such as morphological, hydrological, geographical and anthropogenic factors, however precipitation is the most significant among them.

Materials and Methods>

This manuscript is a documentation of the methods used to calculate land use areas for Shkumbini WEAP catchments. Various land use areas can generate specific run-off, however certain land use types permit the intensive rainfall to become instantaneous streamflow. Other areas may retain water and release it gradually, producing a constant run-off even during periods of low rainfall. The watershed elements in the WEAP model allow us to compute the areas of different land use types within a catchment and specify their corresponding hydrology through calibration process. Once the values for land use parameters have been obtained and organized, future scenarios can inspect the outcomes of land use change. To calculate land use by watersheds, the follwing elements are needed: a land cover vector file appropriately projected for Albania (WGS84, UTM Zone 34N), a table with the land use types (ex. Corinne's categories), and an already prepared vector/shape file with the boundaries of the Shkumbini subbasins (Figure 3 and Table 1).

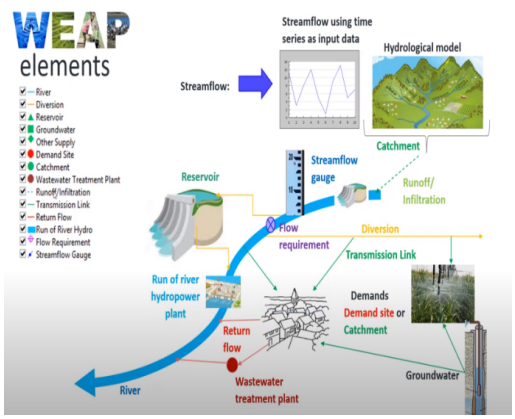

Figure 2. The main components incorporated in WEAP model; source: SEI, 2016.

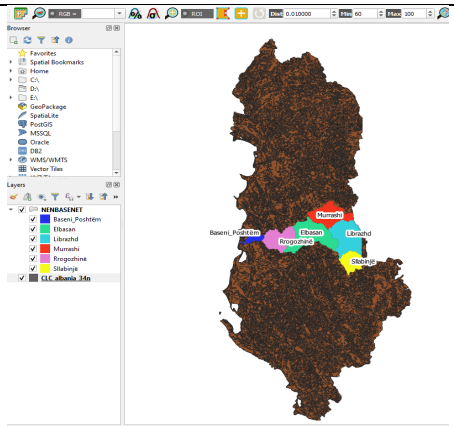

Figure 3. Land Cover vector file projected for Albania in WGS84, UTM Zone 34N and the Shkumbini subbasins in QGIS software.

A vector represents an area using points, lines, and polygons. Vector models are useful for storing data that has discrete boundaries, such as country borders, streets and land use. Vectors can hold many different categories and respective values, which can be viewed in the attribute table. On behalf of this study the watershed delineation of the Shkumbini river basin is performed, derived from a DEM (Digital Elevation Model) via utilization of the QGIS software (Figure 3). The Shkumbini surface area for the six subbasins is provided in the Table 1.

ID	Shkumbini River watersheds	Area (km²)
1	*Sllabinjë*	248
2	*Librazhd*	586
3	*Murrashi*	448
4	*Elbasan*	668
5	*Rrogozhinë*	*391*
6	*Baseni_Poshtëm*	*123*

Table 1. Shkumbini watersheds/ subbasins surface area.

Land cover data was provided by ASIG, the relevant institution in Albania providing the geospatial data and services (ASIG, 2021). The informacion was derived from the EU CORINE 2012 dataset, collected during the calibration period of the model (1991-2016). The CLC2012 file comes with a styled file (clc_legend.qml) which is a QGIS styling file (Figure 4. a, b).

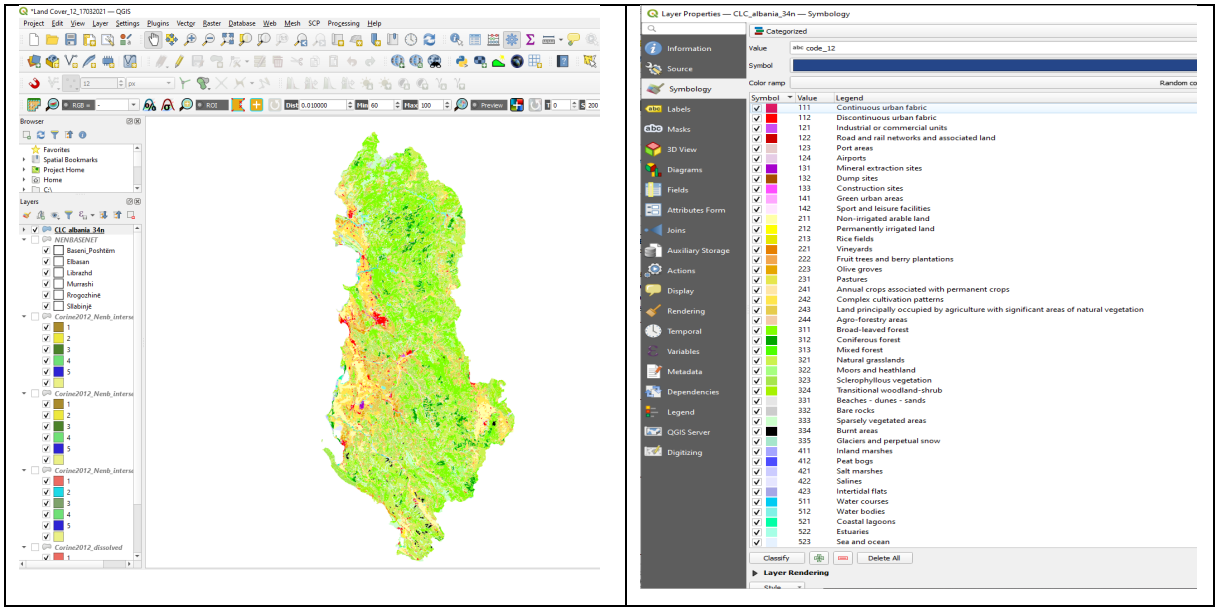

Figure 4. a) Albanian Land Cover 2012 classification in WGS 1984 UTM Zone 34N; b) The symbology of CLC_2012 of Albania in QGIS.

This dataset provides 44 land cover classes at a scale of 1:100 000 for years 2000, 2006 and 2012. The minimum mapping unit of CORINE is 25 hectars (ha). Five meta categories in CORINE are "artificial surfaces", "agricultural areas", "forest and semi-natural areas", "wetlands", "water bodies". For input into the Shkumbini WEAP model, the classification values of the 2012 CORINE dataset were simplified into 10 types (Table 2) (where N/A means that the value did not show up in the Shkumbini watershed).

The first step in land use area calculation concerns selecting the land use types for Shkumbini river basin. The Corinne dataset (available for Albania) comes with 41 different land use types (Level 3), aggregated into 19 categories (Level 2) and 5 meta-categories (Level 1). However, not all of the 51 land use values appear in every area; with regard to the Shkumbini basin, only 44 distinct areas are represented. Using Level 1 categories of the land use types from the Corinne dataset, the following table shows how the land use types are consolidated for this project, totaling 5 different land use types.

Code	CORINE Land Use	Shkumbini WEAP Land Use
1	Continuous urban fabric	Artificial, non-agricultural vegetated areas
2	Discontinuous urban fabric	Artificial, non-agricultural vegetated areas
3	Industrial or commercial units	Artificial, non-agricultural vegetated areas
4	Road and rail networks and associated land	Artificial, non-agricultural vegetated areas
5	Port areas	N/A
6	Airports	Artificial, non-agricultural vegetated areas
7	Mineral extraction sites	Artificial, non-agricultural vegetated areas
8	Dump sites	N/A
9	Construction sites	Artificial, non-agricultural vegetated areas
10	Green urban areas	N/A
11	Sport and leisure facilities	Artificial, non-agricultural vegetated areas
12	Non-irrigated arable land	Arable land
13	Permanently irrigated land	Arable land
14	Rice fields	N/A
15	Vineyards	Permanent crops
16	Fruit trees and berry plantations	Permanent crops
17	Olive groves	Permanent crops
18	Pastures	Pastures
19	Annual crops associated with permanent crops	Heterogeneous agricultural areas
20	Complex cultivation patterns	Heterogeneous agricultural areas
21	Land principally occupied by agriculture, with significant areas of natural vegetation	Heterogeneous agricultural areas
22	Agro-forestry areas	N/A
23	Broad-leaved forest	Forests
24	Coniferous forest	Forests
25	Mixed forest	Forests
26	Natural grasslands	Scrub and/or herbaceous vegetation associations
27	Moors and heathland	Scrub and/or herbaceous vegetation associations

28	Sclerophyllous vegetation	Scrub and/or herbaceous vegetation associations
29	Transitional woodland-shrub	Scrub and/or herbaceous vegetation associations
30	Beaches, dunes, sands	Open spaces with little or no vegetation
31	Bare rocks	Open spaces with little or no vegetation
32	Sparsely vegetated areas	Open spaces with little or no vegetation
33	Burnt areas	N/A
34	Glaciers and perpetual snow	N/A
35	Inland marshes	Wetlands
36	Peat bogs	N/A
37	Salt marshes	Wetlands
38	Salines	N/A
39	Intertidal flats	N/A
40	Water courses	Waters
41	Water bodies	Waters
42	Coastal lagoons	N/A
43	Estuaries	N/A
44	Sea and ocean	N/A
48	NODATA	N/A
49	UNCLASSIFIED LAND SURFACE	N/A
50	UNCLASSIFIED WATER BODIES	N/A
255	UNCLASSIFIED	N/A

Table 2. CORINE Land use classes in 2012 (left) and WEAP generalized land use classes (right)

After some styling edits in QGIS and making the subbasins transparent:

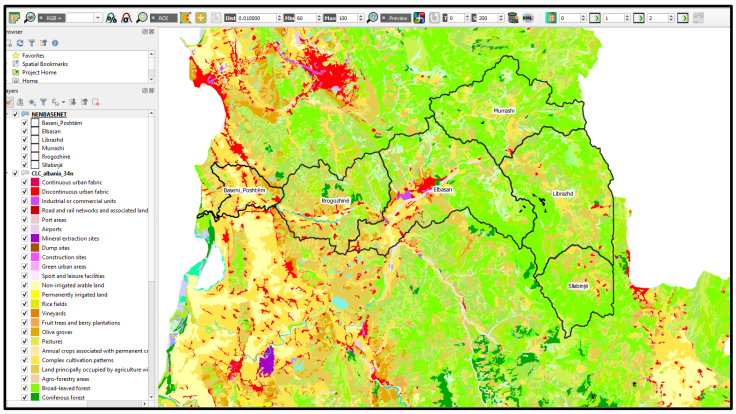

Figure 5. Shkumbini watersheds borders in QGIS (in the background is Albanian CLC_12 shape file).

For the aggregated land cover classes, the derived percentages should be fixed for each of the polygons. After applying Intersect algorithm in QGIS of the Corine land use/land cover classes with the subbasins, is then possible to calculate the class area of the intersected result. Then the proportion with the catchment

area can be calculated, resulting in percentage per class according to the WEAP format. The new shape file is saved in the working environment in QGIS. The area is reduced as shown in Figure 6.

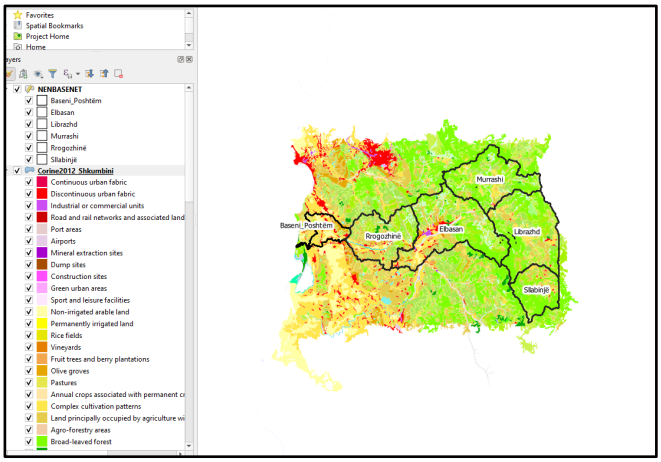

Figure 6. The interested area after applying Intersection in QGIS.

Level 3 of the Corine 2012 classes should be aggregated into the Level 1 which reduces the land cover in five classes. At the attribute table a new column is created with the name Level 1 (1 digit). This can be done through utilization of Expresion Dialog ne QGIS building up the formula as showing in the Figure 7.

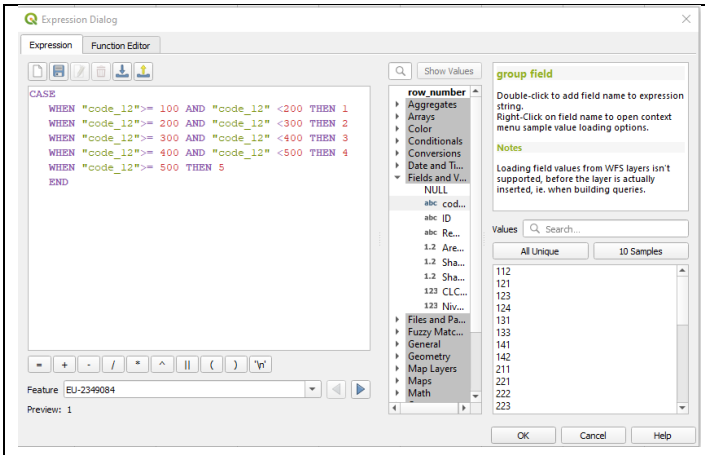

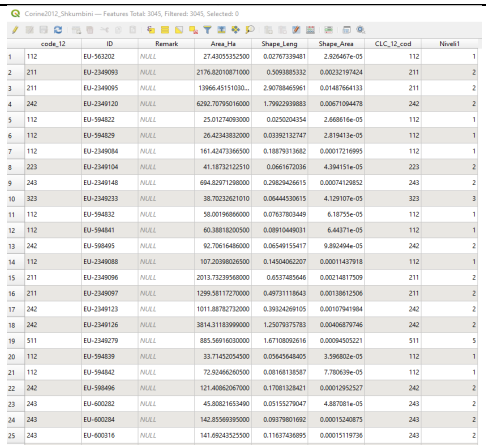

Figure 7. a) Expresion Dialog for Land cover aggregation from Level 3 to Level 1 of the CLC_2012.

b) Attribute table after aggregation

After saving the file, the Dissolve function was applied because there will be many polygons having the same land cover class; this should be considered as one Feature (Figure 8).

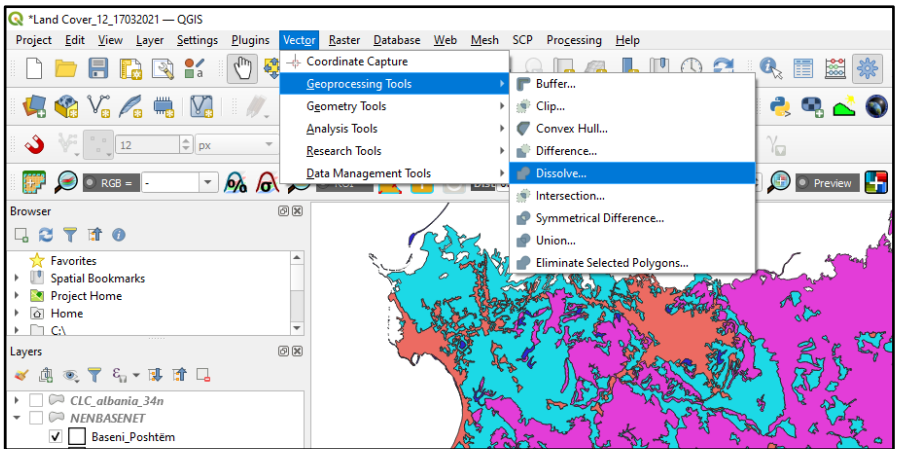

Figure 8. Applying Dissolve function based in the Level 1 of the CLC 2012.

The dissolved file is saved and the land cover classification is aggregated based on Level 1 field; as an example each polygon with number 1 will become one Feature and so on. Therefore, there is a reduction in the Corine land cover into five classes (1-5) as shown in the Figure 9.

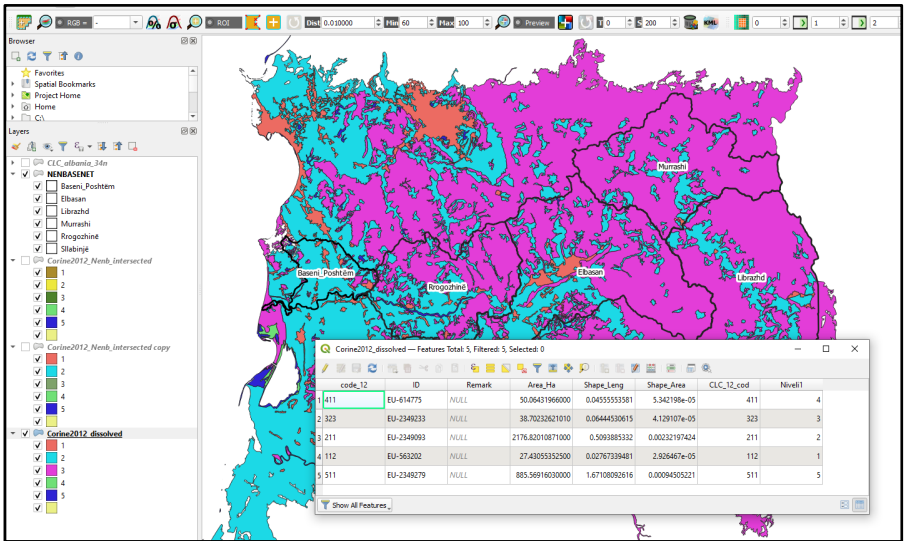

Figure 9. Dissolved Land cover into the Level 1 of the CLC_2012 (5 classes).

If we apply again the Intersection algorithm of the five Corine land cover classes with the Shkumbini watershed polygons, then it is possible to have the percentage of each of the classes in each of the subbasin/watershed. The output was saved (Figure 10. a,b).

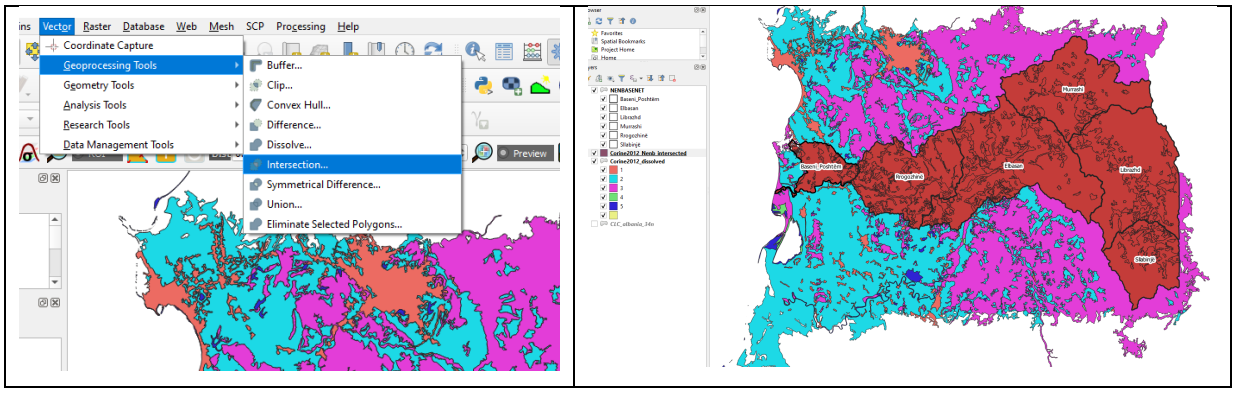

Figure 10. a) Browsing for applying Intersection of the polygon watersheds with the CLC 2012 classes.	*b) The intersected polygons*

Figure 11 shows only the Land Cover in the Shkumbini cachments, reduced into the five classes after applying the same styling as before in QGIS, so that each value represents a point in a spectrum of 1-41 using a color ramp.

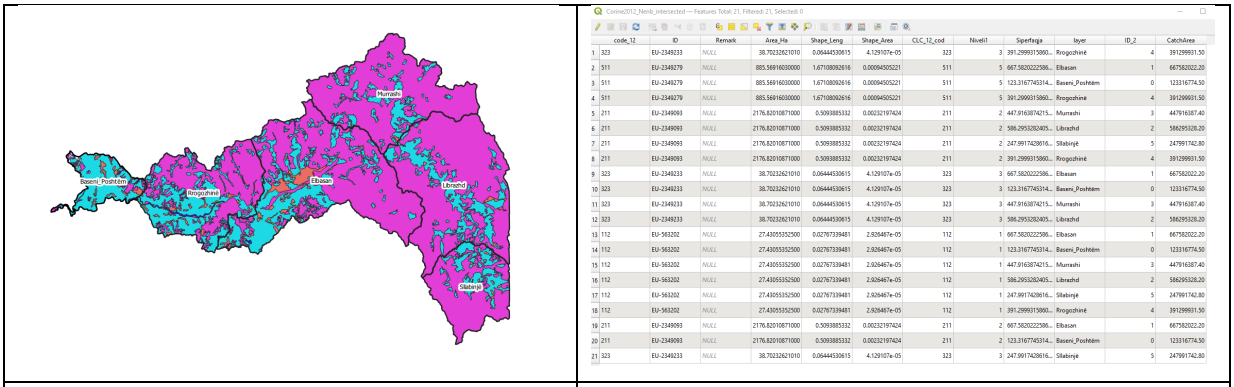

Figure 11. a) Corine Land Cover classes in each of the Shkumbini subbasins	*b) The attribute table of the Corine Land Cover classes*

In the Attribute table of the new vector file, a new field should be added, as it is necessary to know the area of each Feature, calling it class area. Execution of the $area function in the Field Calculator makes it possible to find the area of each of the Level 1 of the CLC 2012 classes in each of the subbasins. The final step is finding the proportion and calculating the percentage that each class does occupy in each of the subbasin. For that a new field needs to be added in the Attribute Table (calling it Percentage). In the Expresion Dialog, through the formula (ClassArea/CachArea)*100 the percentage is calculated and the results are shown in the Figure 12 (*Perqindja* means Percentage).

layer	ID_2	CatchArea	ClassArea	Perqindja
Baseni_Poshtëm	0	123316774.50	11609912.41	9.4
Elbasan	1	667582022.20	35312054.03	5.3
Librazhd	2	586295328.20	4478906.42	0.8
Murrashi	3	447916387.40	1105269.40	0.2
Rrogozhinë	4	391299931.50	12721435.10	3.3
Sllabinjë	5	247991742.80	3543887.26	1.4
Baseni_Poshtëm	0	123316774.50	95809121.95	77.7
Elbasan	1	667582022.20	205244340.80	30.7
Librazhd	2	586295328.20	121861596.30	20.8
Murrashi	3	447916387.40	74759697.99	16.7
Rrogozhinë	4	391299931.50	166208907.50	42.5
Sllabinjë	5	247991742.80	62904201.63	25.4
Baseni_Poshtëm	0	123316774.50	12879155.54	10.4
Elbasan	1	667582022.20	425813492.80	63.8
Librazhd	2	586295328.20	459954822.30	78.5
Murrashi	3	447916387.40	372051419.90	83.1
Rrogozhinë	4	391299931.50	208063910.70	53.2
Sllabinjë	5	247991742.80	181543660.80	73.2
Baseni_Poshtëm	0	123316774.50	789856.02	0.6
Elbasan	1	667582022.20	1212134.81	0.2
Rrogozhinë	4	391299931.50	4305673.94	1.1

Figure 12. Percentage of each CLC 2012 class in each of the Shkumbini subbasin.

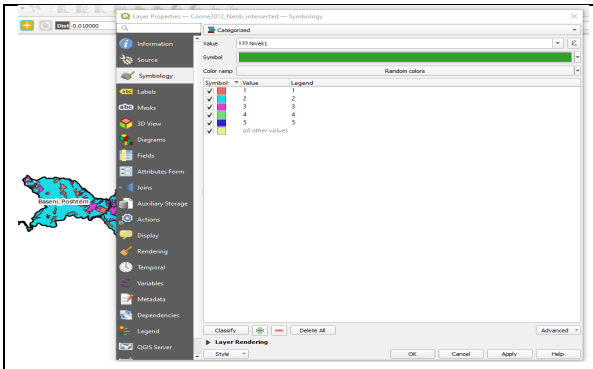

Figure 13. a) Naming of the five classes according to Corine 2012 legend sld file.

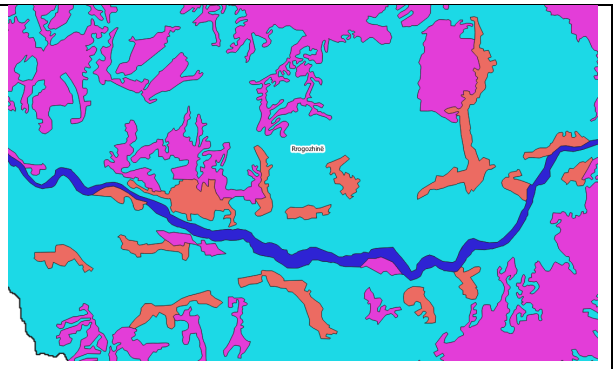

b) View of the Corine Land Cover in the Rrogozhinë subbasin.

Level 1	Name of the (CLC 2012) Classes, Level1
1	Artificial Surfaces
2	Agricultural Areas
3	Forest and Semi Natural Areas
4	Wetlands
5	Water Bodies

Table 3. Name of the (CLC 2012) Classes (1-5), Level1

Sum of Percentage	Column Labels					
Row Labels	**Baseni i Poshtëm**	**Elbasan**	**Librazhd**	**Murrashi**	**Rrogozhinë**	**Sllabinjë**
1 - Artificial Surfaces	9.4%	5.3%	0.8%	0.2%	3.3%	1.4%
2 - Agricultural Areas	77.7%	30.7%	20.7%	16.7%	42.5%	25.4%
3 - Forest and Semi Natural Areas	10.4%	63.8%	78.5%	83.1%	53.1%	73.2%
4 - Wetlands	0%	0%	0%	0%	0%	0%
5 - Water Bodies	2.5%	0.2%	0%	0%	1.1%	0%
Grand Total (%)	**100%**	**100%**	**100%**	**100%**	**100%**	**100%**

Table 4. Percentage of each CLC 2012 class in each of the Shkumbini subbasin.

Table 4 shows the final results in the Percentage form for each CLC 2012 class in every individual Shkumbini subbasins as it is required in the WEAP format (SEI, 2016).

RESULTS AND DISCUSSION

This article conveys a summary of the generalized land cover type distribution for the entire Shkumbini basin and details the methods used for its calculations. From the data presented it is clear that relatively natural land cover types dominate, mainly because of the changing topography and inaccessibility of the Shkumbini river basin. Different land use areas can produce various run-off. This means that some areas may be "flashy" so that important rainfall becomes immediate discharge, but other land use types may retain water and release it slowly, creating a steady run-off even during periods of low rainfall.

The Albanian Land Cover 2012 shapefiles are in WGS 1984, UTM Zone 34N. Using the open source QGIS software, the CORINE land use data were summarized and aggregated to the delineated WEAP catchment objects.

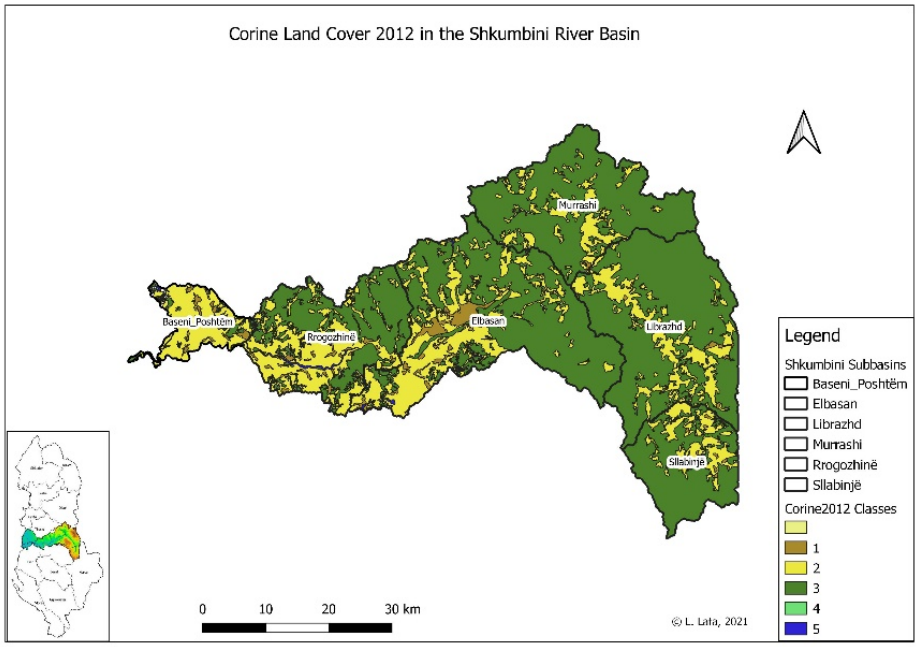

Figure 14. Level 1 Classes of the Corine Land Cover 2012.

The watersheds of the Shkumbini WEAP model were obtained on behalf of this study based on the streamflow gauges used as calibration points. The watershed delineation divides the water production within WEAP (in watershed nodes) into areas that match the subbasins above the specific streamflow gauges. This approach permits for direct water flow comparison, in the current model of Shkumbini river, to the historic data observed at the hydrological stations.

Considering the Papër streamflow gauge as an example, the tan region on the map represents the area where precipitation flow would be directed into the river section between the upstream gauge in Murrashi and the Papër streamflow gauge. The water measured at the streamflow gauge in Papër can be derived through the following equation:

Flow at Papër = Upstream Gauge Values (river flow at Murrashi) + Immediate Upstream Additional flow (Elbasan catchment inflow) – Immediate Upstream

Where "immediate upstream" means WEAP nodes physically located in the tan catchment area upstream of the Papër stream gauge (Figure 15).

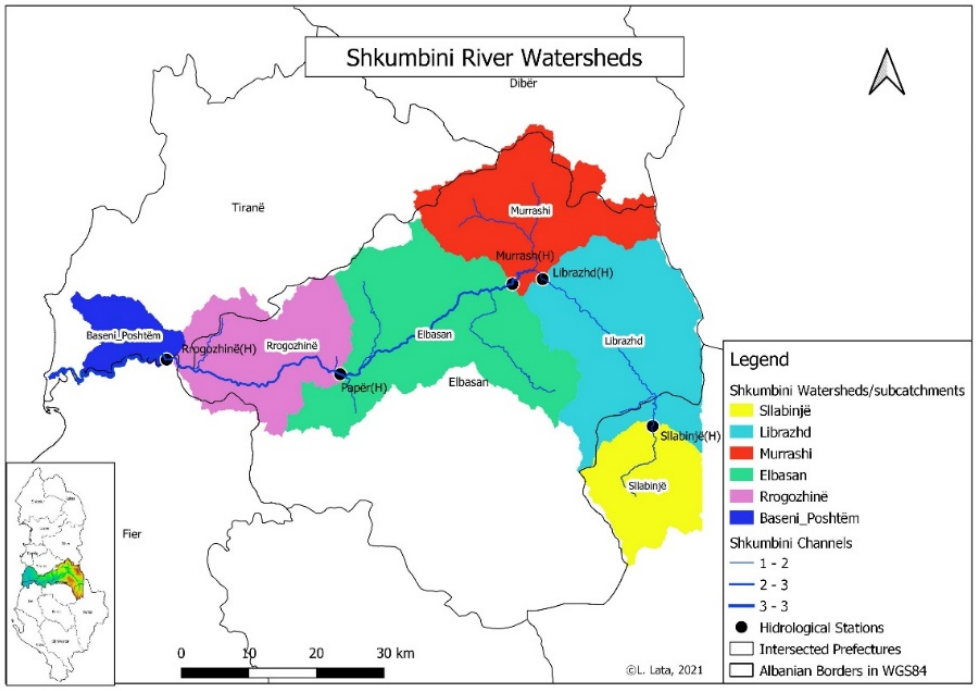

Figure 15. Shkumbini delineated catchments for the WEAP model; source: own elaboration.

The catchment was delineated using the GIS software with the SAGA Tools extension and a Digital Elevation Model (DEM); the final Shkumbini watersheds shape files have been used in the WEAP model for further analysis (Figure 16).

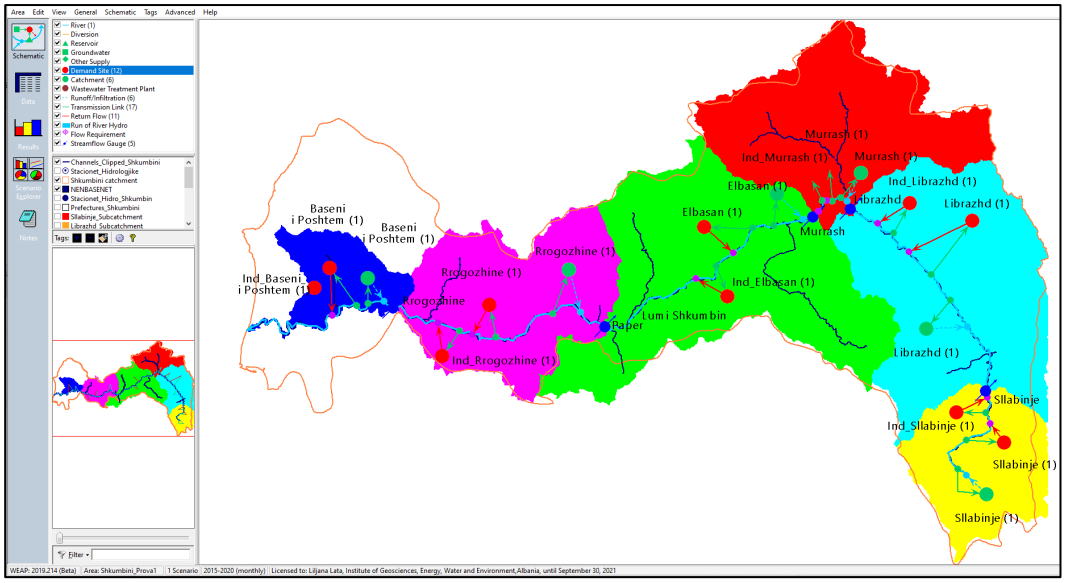

Figure 16. WEAP model schematic; source: own elaboration.

Eventually, all the model parameters are calibrated for the period during which there are historic records for both meteorological data (temperature and precipitation and relative humidity) and streamflow gauge data (average daily water level). For the Shkumbini river basin, the calibration period is from year 1991 to 2016. The Shkumbini WEAP model has a monthly time step, therefore the average daily data were aggregated into this time step.

Figure 18 shows the aggregated monthly streamflow data for the chosen stations for years 1990 to 1992. The model calibration involves the land use characteristics for catchments upstream of the five monitoring stations that were used to calibrate the model. The calibrated stations are Sllabinjë (upstream catchment: Sllabinjë), Librazhd (upstream catchment: Librazhd), Murrash (upstream catchment: Murrash), Papër (upstream catchment: Elbasan), and Rrogozhinë (upstream catchment: Rrogozhinë). The uncalibrated catchment is Baseni i Poshtëm which is assumed to have the same land use parameters to the closest station geografically, the Rrogozhinë station.

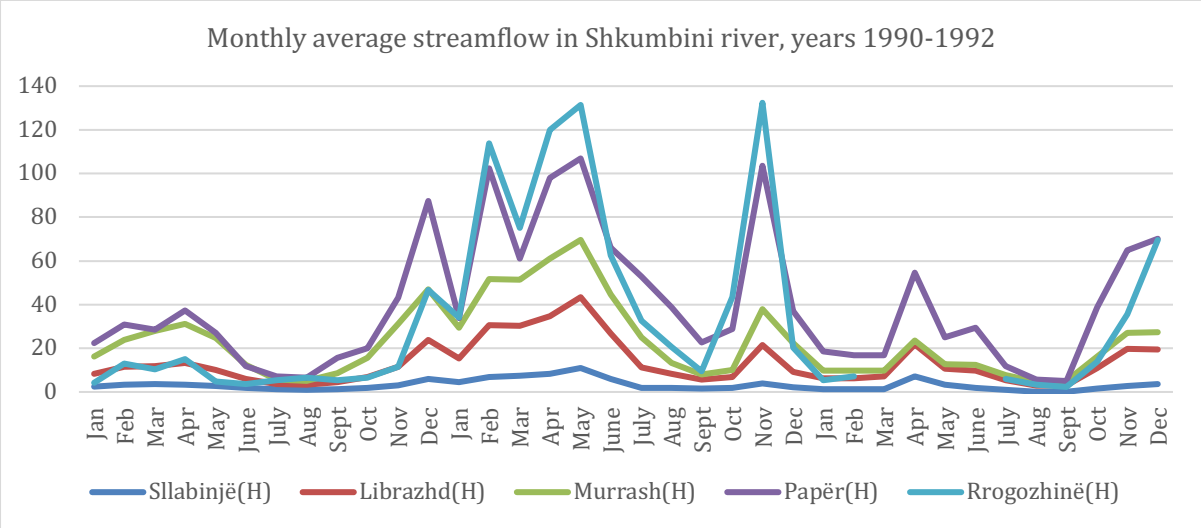

Figure 18. Monthly Streamflow for the chosen Shkumbini hydrological stations (1990-1992).

The catchment elements in WEAP allow us to calculate the areas of different land use types within a watershed and characterize their respective hydrology. Once the values for land use parameters have been established, future scenarios can examine the consequences of land use change.

Additionally, further data preparation and processing procedures were also performed during the study implementation. The resulting suitable data are entered for every element built into the WEAP schematic: water supply (e.g. rivers, reservoirs, etc.) and demand (e.g. drinking water demand, irrigation, industrial water demand, etc.) followed by the model calibration process. Finally, following the WEAP format requirements (SEI, 2016), different climate and development scenarios are prepared with the purpose of effectively representing the natural conditions of the Shkumbini river basin.

CONCLUSION

Collected water demand data for the Shkumbini river basin is structured around three major subsets: Agricultural, Industrial and Urban demand. While some data may not be available, estimates can be made based on derived parameters such as land cover, population census data and general information related to per capita water use. On behalf of this study, Shkumbini River Basin has been divided into six watersheds/subbasins with the purpose of considering as many hydrological stations as possible in the delineation model, avoiding large watersheds. The format of this data must fit the population subdivisions of the model, that were divided according to the delineated catchments. Certainly, the WEAP model outputs and results will have a certain level of accuracy and applicability depending immediately on the available data that describe the complexity of the Shkumbini WEAP system (SEI, 2016).

As the WEAP model uses the Corine dataset, a study on the impact of the land use changes can be performed making use of the WEAP system. However different kind of data are needed to characterize the soil and plant variables for each type of the land use, including soil water capacity, runoff resistance, crop coefficient values etc. The above mentioned data was largely unavailable for the specified land cover of the Shkumbini WEAP model. For this reason the land cover in each of the Shkumbini watersheds share the same quantifications, therefore they can not be distinguished, nor can land use change be studied within the current framework of the existing model. Nevertheless it is possible to examine the runoff related consequences in the Shkumbini basin, in a land use change scenario when considerably less runoff is available to discharge into the river due to the increased possibility of soil infiltration, evaporation and other water loss causes such as reforestation occurence. The examination can be done through the Land Use Change scenario by increasing the values of “Runoff Resistance Factor” for all land use types. This parameter, which varies sesonally, indicates the amount of precipitation that is converted into runoff, as opposed to the amount that infiltrates into the ground. The runoff resistance factor varies from 0 to 1000 (0 indicates that the entire precipitation turned into runoff, whereas 1000 indicates that no runoff occurs only infiltration). This parameter is very low for the Shkumbini river basin because of the steep mountain slopes in the upper part of the river basin particularly. This issue however (increasing the runoff resistance factor) is a subject of an ongoing study related to land use changes in non-irrigated natural environments.

REFERENCES

ASIG, 2021. *ASIG Geoportal:* https://geoportal.asig.gov.al/en, Tirana, Albania

IHM, 1984. Hydro -Meteorological Institute of Albania (IHM), *Hydrology of Albania,* Tirana, Albania.

IHM, 1985. Hydro - Meteorological Institute of Albania (IHM), *Climate of Albania,* Tirana, Albania.

INSTAT, 2011. Statistical Yearbook, Census in Albania. INSTAT, Tirana, Albania.

Agrotec, 2017. *Technical assistance for institution building of the Ministry of Environment in enforcing environmental and climate Acquis,* The European Union’s IPA 2013 Programme for Albania (EuropeAid/135700/DH/SER/AL).

Lata, L. 2020. *Catchment Delineation for Vjosa River WEAP model, using QGIS Software*. Journal of International Environmental Application and Science, 15 (4) , 203-215 . Retrieved from https://dergipark.org.tr/en/pub/jieas/issue/58720/840464

Lata, L., Bart, AJ. Wickel., Galaitsi, S., Samper Hiraldo, A., Bruci, E., 2018. *First assessment of the impacts of climate change and development on the water resources of the Vjosa River, Albania.* Proceedings of ICOALS. Conference date: May 07-09, 2018. Agricultural University of Tirana.

Bruci, E., 2020. *Report on climate change scenarios for the Shkumbini River Catchment area.*

QGIS User Guide: https://docs.qgis.org/2.18/pdf/en/QGIS-2.18-UserGuide-en.pdf

QGIS download*:* https://www.qgis.org/en/site/

SEI, 2016. *WEAP Tutorial*: https://www.weap21.org/downloads/WEAP_Tutorial.pdf

Wickel, B., Lata, L., Galaitsi, S., Hiraldo, A.S., Bruci, E., 2017. *Assessment of Hydro-Ecological and Socio-Economic Systems of the Vjosa River*, under the EU Flood Protection Infrastructure Project – FPIP.

A SUSTAINABLE APPROACH: EVALUATION OF WASTE ECOLOGY AND CONSTRUCTION WASTE

REFİA GÜNGÖR, GÜRAY YUSUF BAŞ, NİHAN ENGİN

Refia Güngör, Research Assistant, Kilis 7 Aralık University, **Güray Yusuf BAŞ**, Research Assistant, Karadeniz Technical University, **Nihan ENGİN**, Professor Doctor, Karadeniz Technical University

Abstract

With the development of the industry, technology has advanced and the human population has increased rapidly in a short time. The rapid increase has necessitate raw material and energy consumption in every sector. In addition, it has caused the occurrence of various wastes. Waste is defined as any substance / material that is dumped, left or must be disposed of by the producer or the person who actually owns the object.

Waste poses a threat to a sustainable world but it is an opportunity for sustainable development strategies. Sustainable development strategies aims to protect the planet and to ensure the well-being of living creatures who live in present and future. For this purpose, wastes are seen as a potential new raw material and energy source, not as a stack that affects human health and needs to be disposed of. The target is to reduce the amount of waste and to utilize the waste generated. 5 different methods are applied to utilize the waste potential. The first method is to minimize the amount of materials, objects or raw materials in the usage process to prevent waste generation (Reduce). The second method is to restore the material, object and a product that has lost its function by repairing it or taking it apart (Reuse). The third method is to make unusable materials or objects part of a whole with different or the same function (Recycle). The fourth method is to process materials that can no longer be used and turn them into energy (Recovery). The fifth method is the disposal of materials that are considered to be of no benefit.

Waste is divided into various sub-categories such as urban, agricultural, industrial, mineral, domestic and construction waste. Among these categories, construction and demolition wastes constitute the most significant percentage. Therefore, construction and demolition waste will be discussed in the study. The aim is to evaluate practices that rationalize the use of construction waste, raw material, energy and contribute to ecological sustainability. Within the scope of the study, the construction waste strategies of the member and candidate countries implementing the European Union Directives were examined; countries' data were analyzed according to the target of the European Union Protocols. As a result of the study, the following evaluations were made; the main factors determining the recycling and recovery rate of construction waste are not parameters such as population and economy, but regulations and targets put into effect; that laws and strategies need to be developed at country and union level; It is critical to raise awareness of the public and institutions on recycling and material use.

Keywords: Sustainability, Ecology, Waste Management, Construction and Demolition Waste

INTRODUCTION

Waste is defined as any substance / material that is dumped, left or must be disposed of by the producer or the person who actually owns the object (T.C. Resmi Gazete, 2015).

The amount of waste is directly proportional to the material used and the human population. Especially after the Industrial Revolution, the amount of raw materials used has increased considerably due to factors

such as the development of the welfare level, the expansion of the human population, destructive wars and so on. In the last century, waste generation has become unsustainable due to excessive population growth and intensive urbanization. For this reason, individuals and administrations have started to take measures according to the type of material by separating the wastes. Waste types that occur in cities are divided into 8 groups (Karakaya Çelik, 2019; URL-1):

Residential: food, textiles, plastics etc.

Industrial: Light and heavy manufacturing, fabrication etc.

Commercial: hotels, restaurants, markets etc.

Institutional: schools, hospitals etc.

Construction and demolition: construction sites, road repair, demolition of buildings etc.

Municipal services: street cleaning, landscaping, parks etc.

Process: refineries, chemical plants, power plants etc.

Agriculture: farms etc.

Approximately 15% of urban wastes are construction and demolition wastes (CDW). This rate can rise up to 50% as a result of factors such as natural disasters. In addition, 40% of the raw materials found in nature are used in construction works (Erdik Aldırmaz, 2018; Karakaya Çelik, 2019). Therefore, CDW will be discussed in this study. The aim is to evaluate practices that rationalize the use of CDW, raw material, energy and contribute to ecological sustainability. Within the scope of the study, the CDW strategies of the member and candidate countries implementing the European Union Directives were examined; countries' data were analyzed according to the target of the European Union Protocols.

2. SUSTAINABLE WASTE STRATEGY

The European Union waste protocol and the Sustainable Waste Strategy (Waste management hierarchy), which is accepted all over the world, are the decisions and actions taken in the process from the first time the material becomes unusable, until the end of the extinction period of this material. The steps of this strategy and process are as follows:

Reduce

Reuse

Recycling

Recovery

Disposal (Figure 1)

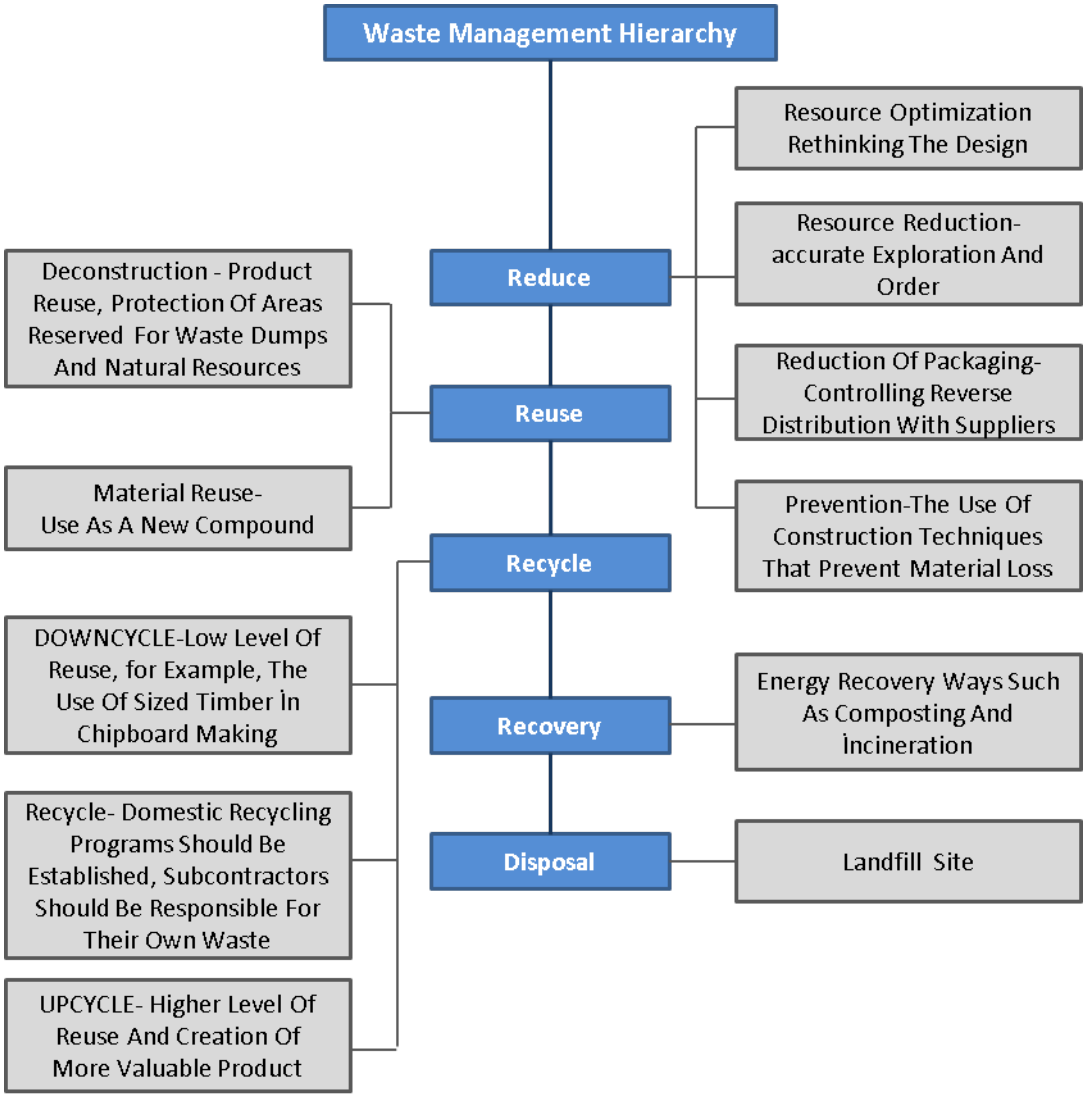

Figure 1. Waste management hierarchy (Ayan, 2013)

The waste management hierarchy refers to a management style that is evaluated from the top to the lowest level and includes certain systems. The most effective principle includes the optimization, prevention and reduction of waste generation. Reduction is possible by considering optimization at the design stage and by using resources correctly and appropriately. Considering certain requirements such as energy, cost, labor, time and technology in waste management, prevention of waste at the first step provides savings in many aspects. It is important to prioritize the higher levels of the hierarchy, as more complex needs emerge from top to down in the waste management hierarchy. The waste management hierarchy steps can be explained as follows:

Reduce; Prevention of waste generation is related to reducing the resource used and this concept constitutes the first step of sustainable waste management. The less waste generated, the less damage it causes to the environment (Keskin, 2018). This method allows for more effective management of other methods used for waste management. The waste prevention method, which reduces the use of materials and raw materials, ensures the protection of natural resources, energy savings, reduction of pollution and waste toxicity ("Sustainable Materials Management," n.d.).

Reuse; the first step of the sustainable waste strategy is to reduce waste generation, but it is not possible to prevent waste generation completely. The waste generated should be evaluated with the most appropriate method in the waste management hierarchy. The reuse strategy, which is in the second step of sustainable waste management, refers to the reutilize of wastes after no or only little processing (Keskin, 2018).

Reusing waste that has not lost its value after use is an effective way to conserve natural resources and save economy ("Sustainable Management of Construction and Demolition Materials," n.d.).

Recycle; The recycling process, which is the third step of sustainable waste management, is defined as the re-inclusion of wastes that can be reused into the production process by subjecting them to various physical or chemical processes (Bozkurt, 2018). Since recycling provides the formation of a raw material, it is important to protect the raw material source to be used in the production of a new material.

Recovery; The process of converting wastes that cannot be reused or recycled into energy is called waste recovery. Waste can be converted into heat, electricity or fuel by techniques such as burning, gasification, pyrolysis, and anaerobic digestion. By converting waste to energy, a renewable energy source is obtained, the use of fossil resources is reduced, and carbon emissions are prevented by reducing the formation of methane gas in landfills ("Sustainable Management of Construction and Demolition Materials," n.d.).

Disposal; The disposal method, which is the last step of the waste management hierarchy, is the disposal of waste that cannot be recycled, reused or recovered in the waste system without harming the society and natüre (Keskin, 2018). The most widely used technique of this method is landfilling (Figure 2). Landfilling is the piling up of waste materials in predetermined areas in a planned or unplanned way. This method is the most economical method known for the disposal of wastes. It is highly used in undeveloped or developing countries (Güleç, 2004).

Figure 2. Landfill practice examples (URL-2 and 3)

3. CONSTRUCTION AND DEMOLITION WASTE (CDW)

The construction sector consumes 16% of fresh water resources, 25% of tree resources, 30% of material resources and 40% of energy resources in construction and operation processes. (Sarıbaş, 2018). These wastes generated by various activities have negative environmental, economic and social effects. Materials that arise due to construction activities and natural disasters and that do not physically contribute to any work after use are called CDW (Bozbeı, 2004). CDW can be in various amounts and percentages in different regions of the world. While this ratio can take different values between 15% and 50% of the solid waste amount in the world; it is on average 36% in the European continent. (Figure 3) (URL-4).

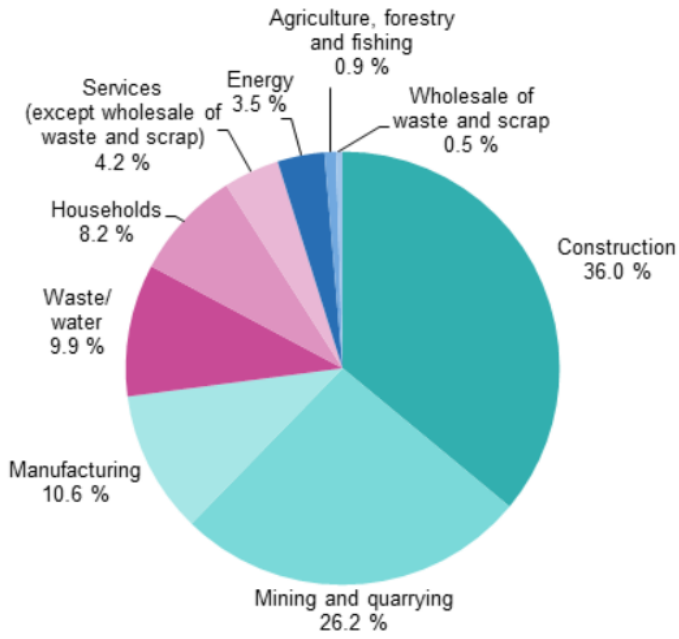

Figure 3. Solid waste rate graph generated as a result of economic activities in the European Continent (URL-4)

CDW can occur in different stages of construction or building use. These wastes can be divided as follows (Ertosun Yıldız, 2017):

The wastes generated during site works before construction (excavation wastes)

The wastes generated during construction

The wastes generated during the use of the building

The wastes generated by the demolition of the building whose service life is over

Nowadays, many countries and unions have adopted various waste management strategies by developing legal regulations and protocols to take precautions against the damages of construction waste. With these waste management strategies, it is aimed to prevent environmental problems and to minimize the carbon footprint of the product in a closed cycle by ensuring material transformation from waste to source. One of the most successful examples of achieving this goal is the European Union practices. The European Union has implemented waste management targets and incentives for countries. The data of the countries aiming to achieve this targets in implementing sustainable waste strategies is presented in the section "3.2. Analysis".

3.1. European Union Construction Waste Management and Strategy

The European Union enacted the "The Waste Framework Directive" numbered 2008/98 EC in 2008 in order to prevent waste generation, protect the environment and human health, and reduce the negative effects of resource use. In this directive, the waste management is constituted by a five-stage "waste hierarchy". In addition, the directive includes targets for 2020 regarding waste management. One of these targets is: "By 2020, the preparing for re-use, recycling and other material recovery, including backfilling operations using waste to substitute other materials, of non-hazardous CDW excluding naturally occurring material shall be increased to a minimum of 70 % by weight." (Directive 2008/98/CE, 2008).

In line with these targets, the European Union has published the “EU Construction & Demolition Waste Management” protocol in 2016, which will contribute to the achievement of the Waste Environment Directive target and provide more recycling. The protocol, developed to be implemented in all member countries of the EU, includes guiding practices for both politicians and institutions. In this protocol, in

addition to the directive adopted in 2008, the responsibilities of the public and private sectors regarding waste generation and management were determined, and recommendations were given on the recycling methods of waste and marketing of recycled materials. The protocol, which is part of the Circular Economy Package, aims to contribute to the correct management of CDW and recycled materials. The reuse, recycling and recovery of CDW have been determined as the priority of the waste management strategy in terms of resource efficiency, sustainability and cost savings within the scope of the determined targets and protocol (European commission, 2016).

Analysis

An additional protocol was published in 2016, which has the same objectives as the directive published in 2008 for the waste recycling targets of the European Union. This Protocol provides information about the implementation methods that can be used to achieve the 2020 waste targets.

Within the scope of this study, the research data conducted in 2010 and 2018 regarding the status of the strategic targets in the process were analyzed for 37 countries. The aim is to compare the status of country data relative to each other and discuss the reasons affecting the results.

Table 1 presents the amount of CDW, population and economic growth rates, which are considered to affect the CDW data for the countries and years identified.

Table 1. Data on waste strategies of European Union member and candidate countries (URL-4)

Countries	**2010 Data**				**2018 Data**			
	Population	GDP and Main Aggregates	CDW (Ton)	CDW Recovery Rate	Population	GDP and Main Aggregates	CDW (Ton)	CDW Recovery Rate
Luxembourg	502 066	40 177.8	8 866 757	98	602 005	60 053.1	7 320 296	98
Ireland	4 549 428	167 673.7	1 609 762	97	4 830 392	326 986.1	1 903 058	100
Norway	4 858 199	2 591 479	1 542 803	44	5 295 619	3 553 900	5 653 304	63
Denmark	5 534 738	1 810 925.6	3 142 215	-	5 781 190	2 253 558	11 999 141	97
Netherlands	16 574 989	639 187	78 063 887	100	17 181 084	773 987	101 661 367	100
Austria	8 351 643	295 896.6	20 927 070	92	8 822 267	385 361.9	48 883 069	90
Iceland	317 630	1 680 966.9	12 289	75	348 450	2 840 088.6	51 034	99
Germany	81 802 257	2 564 400	190 990 217	95	82 792 351	3 356 410	225 260 606	93
Sweden	9 340 682	3 573 581.1	9 381 226	78	10 120 242	4 828 306	12 383 239	90

Belgium	10 839 905	363 140.1	16 852 673	17	11 398 589	460 419.4	22 658 151	97
Finland	5 351 427	188 143	24 645 393	5	5 513 130	233 696	15 715 231	74
France	64 658 856	1 995 289	260 699 131	66	67 026 224	2 360 687	240 207 094	73
United Kingdom	62 510 197	1 606 027	118 910 602	96	66 273 576	2 141 792	137 798 233	98
Malta	414 027	6 815.8	988 070	16	475 701	12 587.4	1 974 801	100
Czechia	10 462 088	3 992 870	9 353 673	91	10 610 055	5 409 665	11 601 305	92
Italy	59 190 143	1 611 279.4	59 340 134	97	60 483 973	1 771 565.9	60 829 199	98
Cyprus	819 140	19 410	461 227	0	864 236	21 432.5	1 053 325	64
Lithuania	3 141 976	28 033.8	356 772	73	2 808 901	45 491.1	620 285	99
Slovenia	2 046 976	36 363.9	1 509 476	94	2 066 880	45 862.6	669 341	98
Spain	46 486 619	1 072 709	37 946 523	65	46 658 447	1 204 241	38 075 987	75
Estonia	1 333 290	14 863.1	436 289	96	1 319 133	25 937.6	2 192 957	95
Poland	38 022 869	1 446 844	20 818 234	93	37 976 687	2 121 555	16 950 306	84
Portugal	10 573 479	179 610.8	1 287 140	58	10 291 027	205 184.1	1 397 749	93
Hungary	10 014 324	27 431 270	4 072 214	61	9 778 371	43 350 353	6 103 907	99
Slovakia	5 390 410	68 188.7	1 786 430	-	5 443 120	89 505.5	541 876	51
Latvia	2 120 504	18 022.7	21 551	-	1 934 379	29 142.5	310 772	97
Romania	20 294 683	528 514.5	734 946	47	19 533 481	951 728.5	647 151	74

Greece	11 119 289	224 124	2 086 080	0	10 741 165	179 727.3	2 286 467	97
Turkey	72 561 312	1 167 664.5	-	-	80 810 525	3 758 315.6	-	-
Croatia	4 302 847	329 431.5	7 656	2	4 105 493	385 376.6	1 259 569	78
Bulgaria	7 421 766	74 434.1	78 880	62	7 050 034	109 743.4	193 186	24
Serbia	7 306 677	3 250 581.3	-	-	7 870 324	5 072 932.2	550 436	81
Montenegro	619 001	3 125.1	-	-	622 359	4 663.1	137 860	-
North Macedonia	2 052 722	437 295.5	-	-	2 075 301	660 878.2	35 617	100
Bosnia and Herzegovina	3 844 046	25 365	-	-	-	33 444.1	122 919	-
Albania	2 918 674	1 239 644.6	-	-	2 870 324	1 635 714.6	-	-
Kosovo	2 208 107	4 402	-	-	1 798 506	6 725.9	-	-

Considering the data in Table 1, in this study, the relationship between the population and CDW, the relationship between economic growth and the amount of CDW, the recycling and recovery rate of CDW are analyzed. These analyzes are as follows:

Relationship between population and CDW amount; population is one of the main factors affecting the amount of CDW. For a sustainable future, it is necessary not only to ensure the waste recycling rate, but also to reduce the amount of waste per person. As a result of the analysis made for this purpose:

Data from 33 of 37 countries has been reached

Population from 33 of 37 countries increased

Per capita CDW rate from 7 of 37 countries decreased, 7 of them remained stable and 19 of them increased (Figure 4).

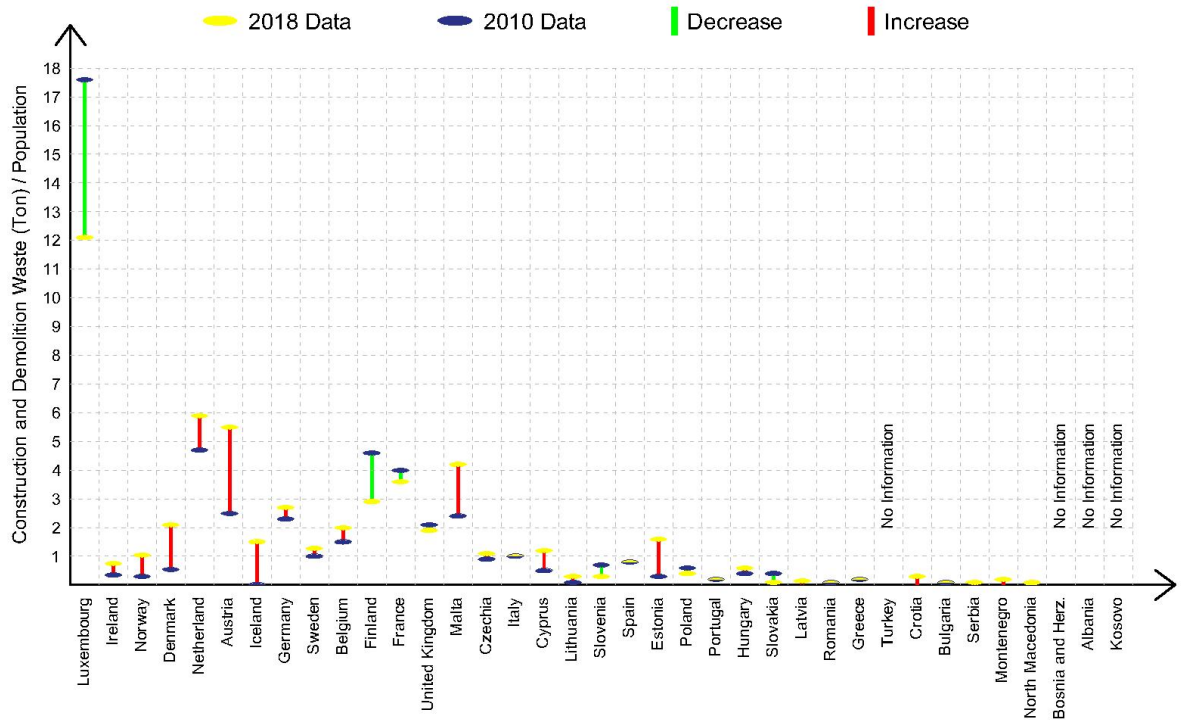

Figure 4. The graph of per capita CDW data compared to 2010 and 2018

Relationship between economic growth and CDW amount; another important issue affecting the amount of CDW is economy. Because one of the main sources of economic development and investment is construction activities. As a result of the analysis on economic growth and the amount of CDW:

Data from 30 of 37 countries has been reached

While the economy of 29 countries had improved, the economy of 1 country had deteriorated,

Among the countries with economic growth, 6 of them decreased the amount of CDW, while 22 of them increased the amount of CDW (Figure 5).

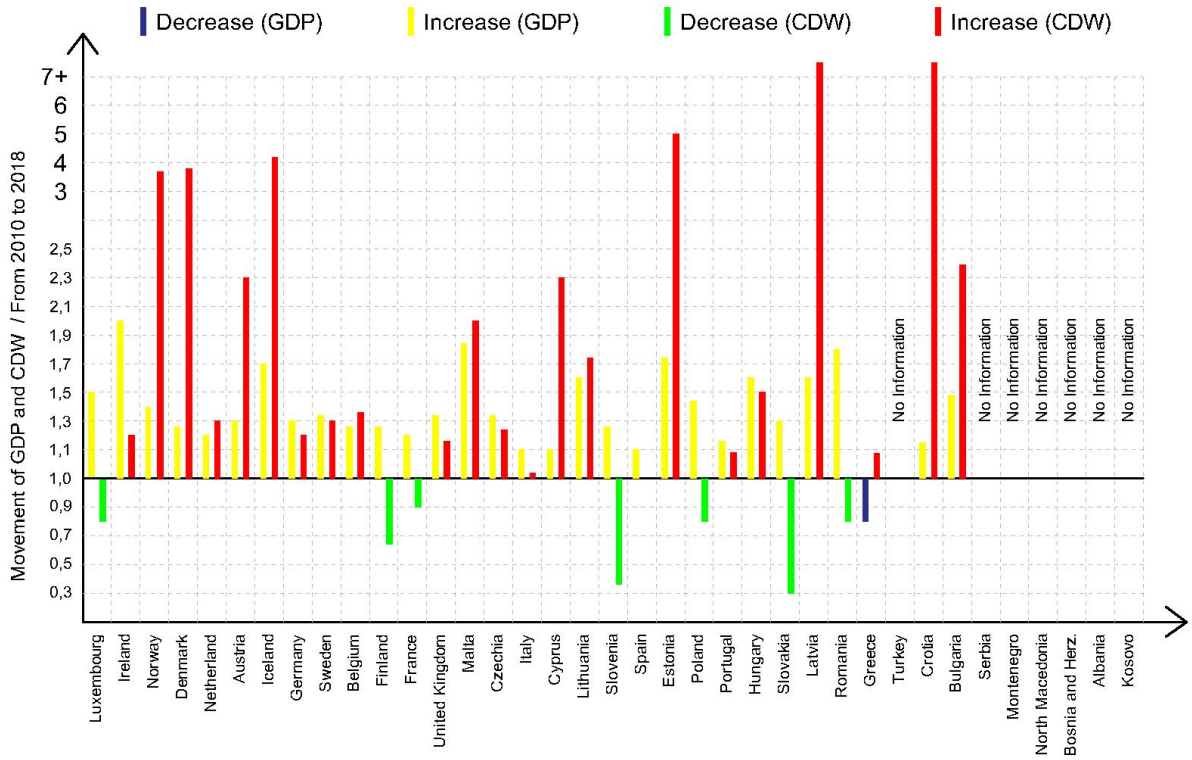

Figure 5. The graph of the change in the economy and CDW amount compared to 2010 and 2018

CDW recycling and recovery rate; in accordance with the protocol of the EU, countries must recycle and recover at least 70% of CDW in 2020. Within the scope of this target, the 2010 and 2018 data of the countries were analyzed and a change graph was created. As a result of the analysis:

Data from 5 of 37 countries hasn't been reached, data from 5 of them are incomplete and data from 27 of them has been reached,

Among these 27 countries, the CDW recycling and recovery rate of 20 countries increased, 5 countries decreased and 2 countries remained stable,

CDW recycling and recovery rate of 28 countries is above the target (70%) (Figure 6).

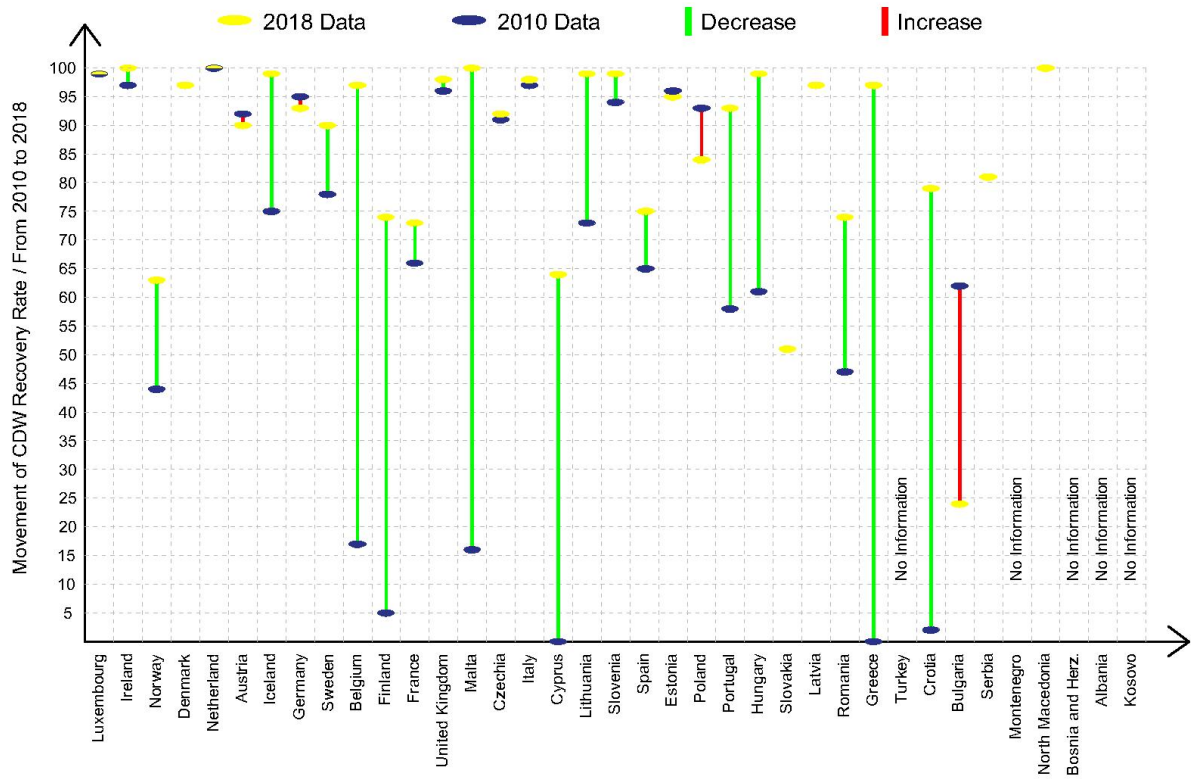

Figure 6. The graph of the change in the CDW recycling and recovery rates of the countries compared to 2010 and 2018

4. DISCUSSION

One of the organizations that set targets and succeed in sustainable waste management is the European Union. When the European Union member and candidate countries are examined, the following can be said in general:

The population of the countries and the amount of CDW are directly proportional.

Among the analyzed countries, the population of 12 countries has decreased, but only 1 of these countries has a decrease in the amount of CDW per capita.

Relationship between CDW and population; The population number is directly proportional to the CDW, but the amount of CDW per capita is determined by the country strategy, not by population increase or decrease.

The relationship between economic development and the amount of CDW differs. Economic development can enable construction activities or construction activities can improve the economy, but there have been many exceptional development differences between the data of them.

In countries with relatively developed economies, the rate of CDW recycling and recovery is generally above average. It is thought that the reason for this may be the initial investment required for recycling (recycling facilities etc.) as well as the country strategy.

The recycling and recovery rate of the CDW of the European Union member and candidate countries is generally high. 75% of the 37 analyzed countries (28 countries) are above the target determined as of 2018. The rate from 3 of the other analyzed countries is in an increasing trend.

The main reason for this data is the incentives for the recycling targets set by the European Union Commission. The European Union Commission has set specific targets for countries. These targets are updated and regulated in certain periods. Countries reaching their targets can carry out R&D studies on waste strategies and establish innovative facilities thanks to the incentives.

5. RESULTS

As long as people continue to exist, they need to produce, and they have to consume. Therefore, waste generation is inevitable. This study aimed to compare the CDW recycling of EU countries and to discuss the reasons that affect the success and failure in this sense. When the methods of the countries that succeeded in this study are examined, the development of the waste strategy and the things to do for CDW can be listed as follows:

Regulations should be arranged at the level of the country or unions, and the relevant institutions and organizations should be authorized to apply.

Waste tax (tax on special wastes such as excavation waste) and its penalty should be regulated as a law,

Responsibilities assigned to public and private organizations should be determined and inspected,

Public and commercial organizations should be raised aware of the use of materials / supplies and the separation of wastes,

Firms or institutions that collect waste should perform this work at different times depending on the type of waste,

Lectures or seminars on effective material and energy use should be given in vocational training.

In order to sustain the ecosystem and provide a livable environment for future generations, human beings should be made conscious on the basis of societies about using raw materials effectively and nature cleanly. The knowledge that develops with awareness should be carefully handled in the construction sector, which constitutes a significant part of the waste generation, and the practices of successful countries in this sense should be an example to others.

REFERENCES

Ayan, A. B., 2013. Dekonstrüksiyon İçin Tasarım Tekniklerinin Türkiye'de Uygulanabilirliği, Master Thesis, İstanbul Technical University, İstanbul.

Bozbeı, H., 2006. İnşaat Atıkları ve Hafriyat Toprağının Ekonomiye Geri Kazandırılması, Master Thesis, İstanbul Technical University, İstanbul.

Bozkurt, H., 2018. Yapısal Atık Yönetimi Bağlamında Yapı Üretiminde Malzeme Seçimi Kriterlerinin Belirlenmesi, Master Thesis. Gebze Technical University, Kocaeli.

Directive 2008/98/CE, 2008, Directive 2008/98/CE of the European Parliament and of the council of 19 November 2008 on waste and repealing certain Directives. Access address: https://eur-lex.europa.eu/legal-content/EN/TXT/?uri=CELEX:32008L0098.

Erdik Aldırmaz, G., 2018, Türkiye'de İnşaat ve Yıkıntı Atıkları Yönetim Sisteminin Mevcut Durumunun Değerlendirilmesi, Master Thesis, İstanbul Technical University, İstanbul.

European commission, 2016. EU Construction & Demolition Waste Management Protocol. Access address: https://ec.europa.eu/growth/content/eu-construction-and-demolition-waste-protocol-0_en.

Ertosun Yıldız, M., 2017. Sürdürülebilirlik Bağlamında Yapısal Atıkların Değerlendirilmesi Ve Yönetim Modeli Önerisi, Master Thesis, Gazi University, Ankara.

Güleç,S., 2004. Belediyelerde Katı Atık Yönetimi (İl Belediyelerinde Bir Araştırma), Master Thesis, Erciyes University, Kayseri.

Karakaya Çelik, S., 2019, Yapısal Atık Yönetimi Bağlamında Belediyelerin Rolü: Kocaeli İli Örneği, Master Thesis. Gebze Technical University, Kocaeli.

Keskin, M. A. (2018). Kentsel Dönüşüm Projeleri Kapsamında Yapısal Atık Yönetiminin İncelenmesi: İstanbul Fikirtepe Örneği. Master Thesis. Gebze Technical University, Kocaeli.

Sarıbaş, İ., 2018. 'Geri Dönüşüm Agregası İçeren Çevreci Betonun Yapısal Eleman Üretiminde Kullanılması', Doctoral Thesis, İstanbul Technical University, İstanbul.

Sustainable Management of Construction and Demolition Materials, (n.d.). Access address: Sustainable Management of Construction and Demolition Materials | Sustainable Materials Management | US EPA

Sustainable Materials Management: Non-Hazardous Materials and Waste Management Hierarchy, (n.d.). Access address: Sustainable Materials Management: Non-Hazardous Materials and Waste Management Hierarchy | Sustainable Materials Management | US EPA

T.C. Resmi Gazete, Çevre ve Şehircilik Bakanlığı, Atık Yönetimi Yönetmeliği, No: 29314, 02.04.2015

URL-1: https://www.unescap.org/sites/default/files/CH08.PDF

URL-2: http://www.viratrabzon.com/haber/trabzon-camburnu-cop-alaninda-yigma-topraga-cop-deposu-40195.html

URL-3: https://mesogeos.gr/en/municipal-solid-waste-sanitary-landfill-site-of-kozai-ptolemaida/

URL-4: https://ec.europa.eu/eurostat